International Journal of Solids and Structures 46 (2009) 4079–4094

Contents lists available at ScienceDirect

International Journal of Solids and Structures

journal homepage: www.elsevier.com/locate/ijsolstr

Constitutive equations for thermomechanical deformations of glassy polymers

A.G. Varghese, R.C. Batra *

Department of Engineering Science and Mechanics, M/C 0219, Virginia Polytechnic Institute and State University, Blacksburg, VA 24061, USA

ARTICLE INFO

Article history:
Received 4 November 2008
Available online 14 August 2009

Keywords:
Material models
High strain rate
Thermo-viscoplasticity
Material softening

ABSTRACT

Poly-Carbonate (PC) and Poly-Methyl-Methacrylate (PMMA) are lightweight and mechanically tough transparent glassy polymers. Their mechanical behavior at low to moderate strain rates has been well characterized; however, that at high strain rates needs additional work. We propose two modifications to existing pressure-dependent viscoplastic constitutive equations that enable one to simulate better mechanical deformations of PC and PMMA at high strain rates. First, the elastic moduli are taken to depend upon the current temperature and the current effective strain rate. Second, two internal variables are introduced to better characterize the strain softening of the material at high strain rates. A technique to find values of newly introduced material parameters is described. We compute the local temperature rise due to energy dissipated during plastic deformations. The true axial stress vs. the true axial strain curves in uniaxial compression from numerical simulations of the test configurations at high strain rates using the proposed constitutive equations are found to agree well with the experimental results available in the literature.

1. Introduction

Several investigators have tested glassy polymers like PC and PMMA experimentally in uniaxial compression (e.g. see Mulliken and Boyce (2006) and Chen et al. (2002)), and constitutive relations have been proposed to simulate their mechanical deformations. Numerical simulations using the constitutive relations proposed by Mulliken and Boyce (2006) replicate well the axial stress vs. the axial strain curves from experimental data for a PC during isothermal deformations and for a PMMA at very low strain rates. However, during high strain rate deformations of glassy polymers, the plastic work is converted to heat (Rittel, 1999). With the Mulliken–Boyce constitutive relations, there are significant differences between results of numerical simulations with the consideration of plastic working and experimental results for uniaxial deformations occurring at moderate and high strain rates. We propose the following two modifications to the Mulliken–Boyce constitutive relations to improve upon the agreement between the two sets of results: (i) in the constitutive relation for the Cauchy stress, we change the dependence of the material parameters from the reference temperature and the reference strain rate to that on the current values of the temperature and the strain rate, and (ii) introduce two additional internal variables in the evolution equations for strain softening to simulate more realistically the response of the material at all strain rates. We also describe the methodology to find values of the new material parameters. Whereas these constitutive relations simulate well the material behavior during loading, no comparison between predictions and test results during unloading has been made because of a lack of experimental data for the glassy polymers tested by Mulliken and Boyce (2006). Like the unified constitutive relation proposed by Bodner and Partom (1975), Mulliken and Boyce's constitutive equations do not assume a yield surface; thus plastic deformations *can* occur at all times. The modified constitutive equations simulate well the mechanical response of glassy polymers over a large range of strain rates.

The rest of this paper is organized as follows. Experimental results of mechanical tests on glassy polymers are first described, and are compared with those from numerical simulations of these tests using the Mulliken and Boyce constitutive relations. We then describe the two modifications to Mulliken and Boyce's constitutive relation to better simulate the response of glassy polymers at moderate to high strain rates. The response of glassy polymers computed with the modified constitutive relation is found to agree well with the corresponding test results of Mulliken and Boyce (2006) and Richeton et al. (2007).

2. Review of experimental results

Results of Dynamic Mechanical Analysis (DMA-ASTM D4065-06) tests for glassy polymers, i.e., plots of the storage modulus vs. the temperature, and the loss modulus vs. the temperature for various frequencies of the axial compressive load are shown in Figs. 1 and 2 for a PC and a PMMA, respectively. The storage and the loss

* Corresponding author. Tel.: +1 5402316051; fax: +1 5402314574.
E-mail address: rbatra@vt.edu (R.C. Batra).

0020-7683/$ - see front matter © 2009 Elsevier Ltd. All rights reserved.
doi:10.1016/j.ijsolstr.2009.08.006

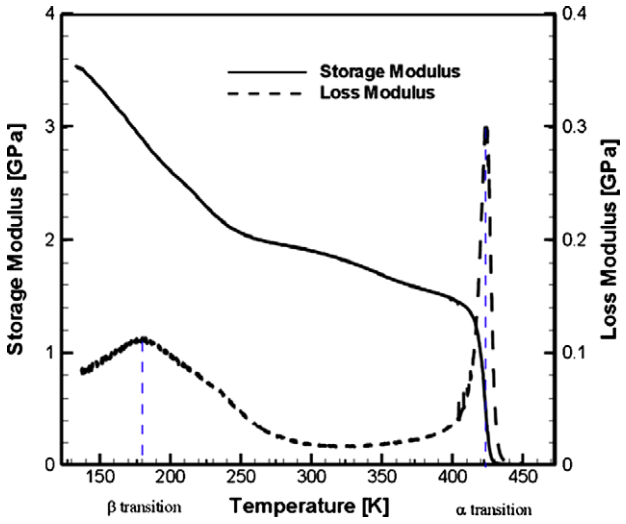

Fig. 1. DMA results for a PC in uniaxial compression at a strain rate of 2.1×10^{-3}/s. Peaks in the loss modulus are at 178 K and 423 K, and correspond to the β and the α transitions, respectively. (*Source*: Mulliken and Boyce (2006).)

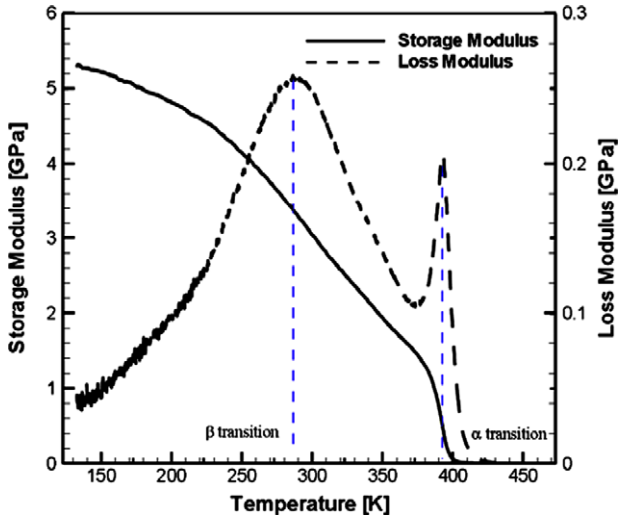

Fig. 2. DMA results for a PMMA in uniaxial compression at a strain rate of 2.1×10^{-3}/s. Peaks in the loss modulus are at 288 K and 388 K, and correspond to the β and the α transitions, respectively. (*Source*: Mulliken and Boyce (2006).)

moduli determine, respectively, the elastic energy stored and the energy dissipated due to viscous effects (Leonov and Prokunin, 1994). Peaks in the loss modulus vs. the temperature curves correspond to transitions that *might* be due to phase changes in the material. Results exhibited in Figs. 1 and 2 depict that the α and the β transition temperatures are closer to each other for the PMMA than those for the PC, and the value of the storage modulus is an order of magnitude higher in the glassy state than that in the rubbery state. Here we focus on developing a constitutive relation for simulating the thermomechanical response of glassy polymers, i.e., polymers below the glass transition temperature.

The pressure and the temperature dependence of the yield stress for a PC (Bauwens-Crowet et al., 1972) and a PMMA (Bauwens-Crowet, 1973) deformed in uniaxial tension and uniaxial compression are shown in Figs. 3 and 4, respectively. We note that the PC and the PMMA tested, respectively, in Bauwens-Crowet et al. (1972) and Bauwens-Crowet (1973) are *not* necessarily the same as those tested by Mulliken and Boyce. For the PC, it was found that the ratio of the magnitude of the yield stress in compression to that

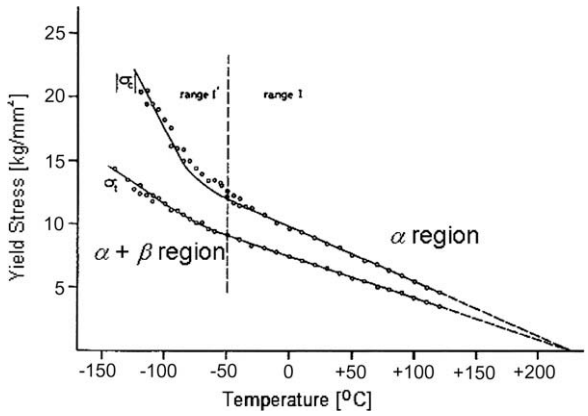

Fig. 3. Yield stress of a PC in uniaxial tension and uniaxial compression as a function of temperature. (*Source*: Bauwens-Crowet et al. (1972).)

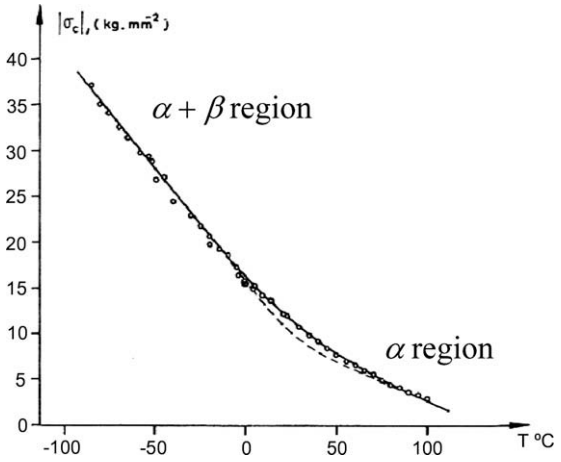

Fig. 4. Variation of the yield stress of a PMMA in uniaxial compression vs. the temperature at an axial strain rate of 4.16×10^{-3}/s. (*Source*: Bauwens-Crowet (1973).)

in tension is a constant over the two ranges of temperatures – the higher temperature (α region) and the lower temperature (($\alpha + \beta$) region). At temperatures below −50 °C, the yield stress was higher than that predicted from the α region which was attributed to the effect of the β phase.

Fig. 4 exhibits the variation of the yield stress of a PMMA in uniaxial compression at an axial strain rate of 4.16×10^{-3}/s over a large range of temperatures. At temperatures below 30 °C (($\alpha + \beta$) region), the yield stress is higher than that predicted from the test results at higher temperatures (α region). Similar results for the yield stress in uniaxial tension for PMMA were not found in the literature because the material was brittle at temperatures lower than 50 °C (Bauwens-Crowet, 1973).

In another set of experiments, the yield stress of a PC and a PMMA in uniaxial compression was found to vary linearly with the logarithm of the axial strain rate (Mulliken and Boyce, 2006; Moy et al., 2003a,b; Boyce and Arruda, 1990), with different slopes in the low to the medium (α region) and the high strain rate (($\alpha + \beta$) region) regimes; cf. Fig. 5.

The true axial stress vs. the true axial strain plots for a PC and a PMMA (Mulliken and Boyce, 2006) in uniaxial compression at various strain rates are exhibited in Figs. 6 and 7, respectively. The stress vs. strain curves for the PC show that the material is ductile in the range of strain rates tested and does not appear to reveal any strain rate dependent softening or hardening. However, the failure

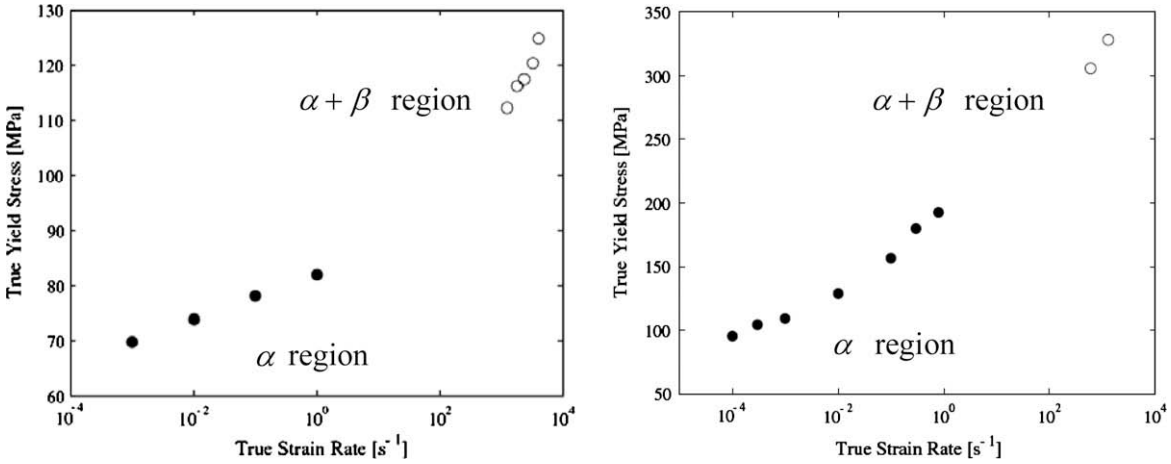

Fig. 5. True yield stress of a PC (left) and a PMMA (right) as a function of the true axial strain rate. (*Source*: Mulliken and Boyce (2006).)

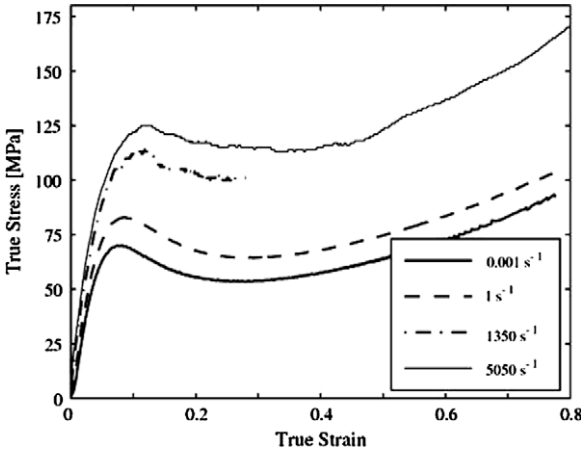

Fig. 6. True axial stress vs. true axial strain for a PC deformed in uniaxial compression at four different strain rates. (*Source*: Mulliken and Boyce (2006).)

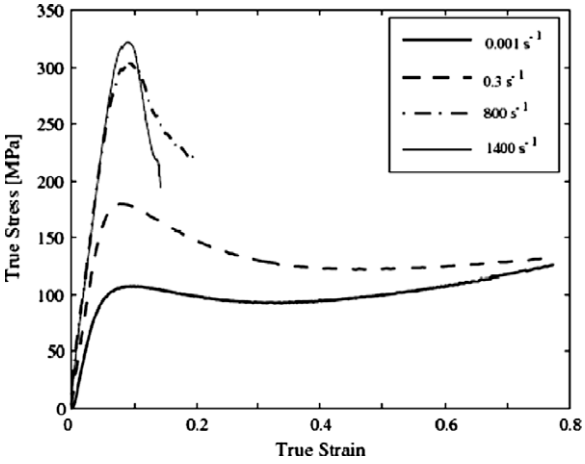

Fig. 7. True axial stress vs. true axial strain for a PMMA deformed in uniaxial compression at four different strain rates. (*Source*: Mulliken and Boyce (2006).)

strain of 0.2 for the PMMA at strain rates exceeding 800/s is considerably less than the strain of 0.8 at strain rates below 0.3/s when experiments were terminated. Furthermore, at strain rates of 800/s and 1400/s, it does not exhibit any hardening following the softening in the post-yield region as it does at strain rates of 0.3/s and 0.001/s.

During unloading the axial stress vs. the axial strain curve is nonlinear for PC (Rittel, 1999) and PMMA (Arruda et al., 1995).

Experimental results other than those summarized above suggest that the mechanical response of glassy polymers also depends on the length of molecular chains, the age, the humidity, the duration of exposure to temperature, ultraviolet radiation, and the chemical environment; however, these effects are not incorporated in the constitutive relation. We focus here on considering the following features of deformations of a PC and a PMMA at different strain rates.

- Temperature, strain rate and pressure-dependent yield.
- Strain softening followed by strain hardening.
- Temperature-dependent viscoplastic deformation.

3. Review of existing constitutive equations

Haward and Thackray (1968) combined an Eyring (1963) and a Langevin spring (Treloar, 1975) to propose a constitutive equation for describing the nonlinear axial stress vs. the axial strain behavior of glassy polymers; it was extended to study three-dimensional (3D) deformations by Parks et al. (1984). Boyce et al. (1988) generalized it to include effects of strain rate, pressure-dependent yielding, strain softening, and temperature. Krempl and Ho (2000) have developed the viscoplasticity based on overstress (VBO) theory to predict the strain rate dependent yielding and loading/unloading behavior of Nylon 66 but not the strain rate dependent softening and the subsequent hardening observed experimentally. Ho and Krempl (2002) extended the VBO theory by introducing an augmentation function that initially decreases and subsequently increases, and reproduces well the rate dependent strain softening and hardening behavior of PMMA at low strain rates. However, they did not compare predictions from the augmented VBO theory with experimental results at high strain rates.

Based on the theory of intermolecular cooperativity Matsuoka (1992) and Frank and Brockman (2001) proposed constitutive equations that account for strain rate, unloading, hydrostatic pressure and strain hardening effects in 3D isothermal deformations of PMMA. However, yielding predicted by these constitutive equations is nearly independent of the strain rate. The axial stress vs. the axial strain predictions from the constitutive equation were compared with experimental data at strain rates of 0.005/s to 6/s. Material parameters were determined by an optimization technique that matches stress vs. strain curves obtained from simulations with those observed experimentally.

Mulliken and Boyce (2006) added an Eyring dashpot to Boyce et al. (1988) constitutive relation to predict the response of glassy polymers at high strain rates and low temperatures. Their constitutive relation can be considered as phenomenological stipulating the co-existence of the following three phases at a material point: an α phase to simulate the mechanical response dominant at high temperatures and low strain rates, a β phase for modeling the mechanical response at low temperatures and high strain rates, and a 'B' phase in which stresses increase exponentially as the stretch reaches a limiting value that is characteristic of the material. The B phase accounts for the strain hardening of the material. The temperature-dependent viscoelastic response is simulated by regarding the two elastic parameters as functions of temperature and strain rate. Additionally, they considered only isothermal deformations of glassy polymers during numerical simulations. The computed axial stress vs. the axial strain curve for uniaxial compressive deformations of the PMMA matched well with that found experimentally at low strain rates but the two curves differed noticeably from each other at high strain rates. The discrepancy between the two curves was attributed to the thermal softening induced during plastic deformations of the PMMA that was not considered in the constitutive relation.

Richeton et al. (2007) proposed constitutive equations for glassy polymers capable of predicting the response of PMMA and PC over a wide range of temperatures and strain rates. The flow rules in the glassy and the rubbery states were based on the cooperative model of Fotheringham and Cherry (1976) and the free volume theory of Williams et al. (1955) respectively. They considered the temperature rise in a PC and a PMMA due to adiabatic heating and material properties like the mass density and the specific heat as functions of temperature. The true axial stress vs. the true axial strain curves predicted from the constitutive relations were found to agree well with the corresponding experimental data from uniaxial compression tests at different temperatures and strain rates. At high strain rates their constitutive equations did not predict well the yield stress and the post-yield behavior of PMMA where additional softening is observed. Experimental observations suggest that PMMA fails due to brittle fracture during high strain rate deformations and hence may not undergo any phase change.

We modify Mulliken and Boyce (2006) constitutive equations to improve upon the correlation between predictions and test results for glassy polymers deformed at moderate to high strain rates in uniaxial compression, and describe techniques to find the two newly introduced material parameters. We first review Mulliken and Boyce's material model, and then discuss the proposed changes. Subsequently, predictions from the modified constitutive relation are compared with test results at different strain rates for uniaxial compressive deformations.

4. Review of Mulliken and Boyce's constitutive equations

We use boldface letters to indicate tensorial quantities. The material response is assumed to be represented by three mechanical systems acting in parallel: phase α, phase β, and phase B (e.g. see Fig. 8). This approach is similar to that of the mixture theory in which all three phases co-exist at a material point. The deformation gradient $\mathbf{F}$ that maps infinitesimal material lines in the undeformed reference configuration to the present configuration is the same for all three phases, i.e.,

$$\mathbf{F} = \mathbf{F}_\alpha = \mathbf{F}_\beta = \mathbf{F}_B \tag{1}$$

Similar to the work of Lee (1969), the deformation gradient for the α and the β phases is multiplicatively decomposed into elastic and plastic parts. That is,

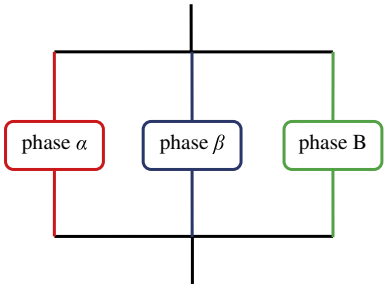

Fig. 8. Schematic depiction of the constitutive equations involving three phases.

$$\begin{aligned} \mathbf{F}_\alpha &= \mathbf{F}_\alpha^e \mathbf{F}_\alpha^p \\ \mathbf{F}_\beta &= \mathbf{F}_\beta^e \mathbf{F}_\beta^p \end{aligned} \tag{2}$$

The plastic deformation gradients $\mathbf{F}_\alpha^p$ and $\mathbf{F}_\beta^p$ map an infinitesimal material line in a stress-free reference configuration to a stress-free configuration obtained by elastically unloading the deformed state of the body. Neither $\mathbf{F}^e$ nor $\mathbf{F}^p$ are gradients of a vector field but $\mathbf{F}$ equals the gradient of $\mathbf{x}(\mathbf{X},t)$ with respect to $\mathbf{X}$.

It is assumed that the plastic deformation is volume preserving, i.e., $\det\mathbf{F}_\alpha^p = \det\mathbf{F}_\beta^p = 1$. While the plastic strains in phases α and β can be computed, the effective plastic strain at a material point cannot be determined using the current kinematic description.

From Eq. (1), it follows that the velocity gradient $\mathbf{L}$, the gradient of $\mathbf{v}$ with respect to $\mathbf{x}$, is also the same in all three phases, i.e., $\mathbf{L} = \mathbf{L}_\alpha = \mathbf{L}_\beta = \dot{\mathbf{F}}\mathbf{F}^{-1}$ where a superimposed dot indicates the material time derivative. The velocity gradient is decomposed into elastic and plastic parts as follows:

$$\begin{aligned} \mathbf{L}_\alpha &= \mathbf{L}_\alpha^e + \mathbf{F}_\alpha^e \mathbf{L}_\alpha^p \mathbf{F}_\alpha^{e^{-1}} = \mathbf{L}_\alpha^e + \widetilde{\mathbf{L}}_\alpha^p \\ \mathbf{L}_\beta &= \mathbf{L}_\beta^e + \mathbf{F}_\beta^e \mathbf{L}_\beta^p \mathbf{F}_\beta^{e^{-1}} = \mathbf{L}_\beta^e + \widetilde{\mathbf{L}}_\beta^p \end{aligned} \tag{3}$$

where $\mathbf{L}^e = \dot{\mathbf{F}}^e\mathbf{F}^{e^{-1}}, \mathbf{L}^p = \dot{\mathbf{F}}^p\mathbf{F}^{p^{-1}}$, and $\widetilde{\mathbf{L}}^e = \mathbf{F}^e\mathbf{L}^e\mathbf{F}^{e^{-1}}$. We assume that

$$\begin{aligned} \widetilde{\mathbf{L}}_\alpha^p &= \widetilde{\mathbf{D}}_\alpha^p + \widetilde{\mathbf{W}}_\alpha^p \\ \widetilde{\mathbf{L}}_\beta^p &= \widetilde{\mathbf{D}}_\beta^p + \widetilde{\mathbf{W}}_\beta^p \end{aligned} \tag{4}$$

where $\widetilde{\mathbf{D}}_i^p$ and $\widetilde{\mathbf{W}}_i^p (i = \alpha, \beta)$ are, respectively, the symmetric and the skew-symmetric parts of $\widetilde{\mathbf{L}}_i^p$; $\widetilde{\mathbf{D}}_i^p$ and $\widetilde{\mathbf{W}}_i^p$ are, respectively, the plastic strain rate tensor and the plastic spin tensor in phase i. Following Mulliken and Boyce we assume that $\widetilde{\mathbf{W}}_\alpha^p = \widetilde{\mathbf{W}}_\beta^p = \mathbf{0}$. Hence it follows from Eqs. (3) and (4) that

$$\begin{aligned} \dot{\mathbf{F}}_\alpha^p &= \mathbf{F}_\alpha^{e^{-1}} \widetilde{\mathbf{D}}_\alpha^p \mathbf{F}_\alpha \\ \dot{\mathbf{F}}_\beta^p &= \mathbf{F}_\beta^{e^{-1}} \widetilde{\mathbf{D}}_\beta^p \mathbf{F}_\beta \end{aligned} \tag{5}$$

The elastic deformation gradient can be determined from Eq. (2) if the total deformation gradient and the plastic deformation gradient are known.

The plastic strain rate tensor is assumed to be coaxial with the deviatoric Cauchy stress tensor. That is

$$\begin{aligned} \widetilde{\mathbf{D}}_\alpha^p &= \dot{\gamma}_\alpha^p \frac{\boldsymbol{\sigma}'_\alpha}{|\boldsymbol{\sigma}'_\alpha|} \\ \widetilde{\mathbf{D}}_\beta^p &= \dot{\gamma}_\beta^p \frac{\boldsymbol{\sigma}'_\beta}{|\boldsymbol{\sigma}'_\beta|} \end{aligned} \tag{6}$$

where $\boldsymbol{\sigma}'_i (i = \alpha, \beta)$ is the deviatoric part of the Cauchy stress $\boldsymbol{\sigma}_i$ in phase i, $|\boldsymbol{\sigma}'_i| = \mathrm{tr}(\boldsymbol{\sigma}'_i\boldsymbol{\sigma}'_i)$ is the magnitude of $\boldsymbol{\sigma}'_i$, tr is the trace operator, and $\dot{\gamma}_i^e$ is the effective plastic strain rate in phase i. It follows from Eq. (6) that

$$\dot{\gamma}_i^p = (\mathrm{tr}(\widetilde{\mathbf{D}}_i^p \widetilde{\mathbf{D}}_i^p))^{1/2} \tag{7}$$

The true strain tensor $\boldsymbol{\varepsilon}$ and the magnitude of the true strain tensor, $\varepsilon_{\mathrm{mag}}$, are defined as

$$\boldsymbol{\varepsilon} = \ln \mathbf{V} \tag{8}$$

$$\varepsilon_{\text{mag}} = \sqrt{\varepsilon_{ij}\varepsilon_{ij}}, \quad i,j = 1,2,3, \quad i \text{ and } j \text{ summed} \tag{9}$$

Here, $\mathbf{V}$ is the left stretch tensor given by $\mathbf{V}=(\mathbf{F}\mathbf{F}^{\mathrm{T}})^{1/2}$.

The Cauchy stresses in the α and the β phases are assumed to be related to their elastic deformations by

$$\begin{aligned} \boldsymbol{\sigma}_\alpha &= \frac{1}{J_\alpha}[2\mu_\alpha \ln \mathbf{V}_\alpha^{\mathrm{e}} + \lambda_\alpha \mathrm{tr}(\ln \mathbf{V}_\alpha^{\mathrm{e}})\boldsymbol{\delta}] \\ \boldsymbol{\sigma}_\beta &= \frac{1}{J_\beta}[2\mu_\beta \ln \mathbf{V}_\beta^{\mathrm{e}} + \lambda_\beta \mathrm{tr}(\ln \mathbf{V}_\beta^{\mathrm{e}})\boldsymbol{\delta}] \end{aligned} \tag{10}$$

where $J_i = \det(\mathbf{F}_i^{\mathrm{e}})$ gives the volume change due to elastic deformations in phase i; $\ln \mathbf{V}_i^{\mathrm{e}}$ is the logarithmic elastic strain in phase i; $\boldsymbol{\delta}$ is the identity tensor, and $\mathbf{V}_i^{\mathrm{e}}$ is the left stretch tensor in the polar decomposition of the deformation gradient $\mathbf{F}_i^{\mathrm{e}}$. The material elasticities λ_i and μ_i (Lame's constants for infinitesimal deformations) are functions of temperature in the reference configuration and the nominal strain rate, and capture the temperature-dependent viscoelastic response of the material.

The Cauchy stress $\boldsymbol{\sigma}_{\mathrm{B}}$ in phase B is assumed to be deviatoric, and given by

$$\boldsymbol{\sigma}_{\mathrm{B}} = \frac{C_{\mathrm{R}}}{3}\frac{\sqrt{N_l}}{\lambda^{\mathrm{p}}} L^{-1}\left(\frac{\lambda^{\mathrm{p}}}{\sqrt{N_l}}\right)\overline{\mathbf{B}}'_{\mathbf{B}} \tag{11}$$

where $\lambda^{\mathrm{p}} = \sqrt{\mathrm{tr}(\overline{\mathbf{B}}_{\mathrm{B}})}/3$ is a measure of stretch; L is the Langevin function defined by $L(\beta)\equiv\coth\beta - 1/\beta$; $\overline{\mathbf{B}}'_{\mathbf{B}}$ is the deviatoric part of $\overline{\mathbf{B}}_{\mathbf{B}} = (\det \mathbf{F})^{-2/3}\mathbf{F}\mathbf{F}^{\mathbf{T}}$ and equals $\overline{\mathbf{B}}_{\mathrm{B}} - (\mathrm{tr}(\overline{\mathbf{B}}_{\mathrm{B}})/3)\boldsymbol{\delta}$; N_{l} is the limiting stretch; $C_{\mathrm{R}}\equiv n_{\mathrm{R}}k\theta$ is the rubbery modulus, θ is the temperature in Kelvin, k is Boltzmann's constant, and n_{R} is a material parameter. The magnitude of the stress in phase B increases exponentially as λ^{p} approaches $\sqrt{N_l}$. For $y=L(x)$;$x=L^{-1}(y)$. Thus the evaluation of $L^{-1}(\lambda^{\mathrm{p}}/\sqrt{N_l})$ involves solving iteratively a nonlinear equation. The magnitude of the Cauchy stress tensor, σ_{mag}, is defined as

$$\sigma_{\mathrm{mag}} = \sqrt{\sigma_{ij}\sigma_{ij}}, i,j = 1,2,3, \quad i \text{ and } j \text{ summed} \tag{12}$$

The total Cauchy stress at a material point equals the sum of Cauchy stresses in individual phases at that point, i.e.,

$$\boldsymbol{\sigma} = \boldsymbol{\sigma}_\alpha + \boldsymbol{\sigma}_\beta + \boldsymbol{\sigma}_{\mathrm{B}} \tag{13}$$

The effective plastic strain rates in α and β phases are taken to be given by

$$\begin{aligned} \dot{\gamma}_\alpha^{\mathrm{p}} &= \dot{\gamma}_{0\alpha}^{\mathrm{p}} \exp\left[-\frac{\Delta G_\alpha}{k\theta}\left(1 - \frac{\tau_\alpha}{s_\alpha + \alpha_\alpha^{\mathrm{p}} p}\right)\right] \\ \dot{\gamma}_\beta^{\mathrm{p}} &= \dot{\gamma}_{0\beta}^{\mathrm{p}} \exp\left[-\frac{\Delta G_\beta}{k\theta}\left(1 - \frac{\tau_\beta}{s_\beta^0 + \alpha_\beta^{\mathrm{p}} p}\right)\right] \end{aligned} \tag{14}$$

Here $\dot{\gamma}_{0i}^{\mathrm{p}}(i = \alpha, \beta)$ is the pre-exponential factor, ΔG_{i} the activation energy, p=-$\sigma_{\mathrm{ii}}/3$ the pressure,$\tau_i = \sqrt{0.5\boldsymbol{\sigma}'_i\boldsymbol{\sigma}'_i}$ the effective stress, α_i^{p} the pressure coefficient, $s_\beta^0 = 0.077\mu_\beta/(1-\nu_\beta)$ the athermal shear strength, ν_{i} Poisson's ratio and s_{i} an internal variable that evolves with plastic deformations. These equations predict the pressure, strain rate, and temperature-dependent evolution of the plastic strain rate in glassy polymers. Since there is no yield surface postulated, plastic deformations always occur. However, henceforth we will refer to the maximum magnitude of the Cauchy stress tensor, σ_{mag}, reached before the onset of material softening as the yield stress of the material.

The internal variable s_α equals the athermal shear strength of phase α, and its evolution is given by

$$\dot{s}_\alpha = h_\alpha\left(1 - \frac{s_\alpha}{s_\alpha^{\mathrm{ss}}}\right)\dot{\gamma}_\alpha^{\mathrm{p}} \tag{15}$$

where h_α is the softening parameter, and s_α^{ss} the preferred state parameter. Eq. (15) implies that $\dot{s}_\alpha$ is almost zero when either $\dot{\gamma}_\alpha^{\mathrm{p}}$ is close to zero or when s_α is close to s_α^{ss}. Hence, the internal variable s_α remains constant during elastic deformations, and evolves during continued plastic deformations to s_α^{ss}. The evolution of s_α simulates strain softening in glassy polymers. The initial value, s_α^0, of the softening variable is given by $0.077\mu_\alpha/(1\text{-}\nu_\alpha)$.

Values of material parameters (Mulliken and Boyce, 2006) for the PC and the PMMA reported by Mulliken and Boyce are listed in Table 1. They proposed that deformations of phase β are affected only by positive pressures. Accordingly, the pressure coefficient $\alpha_\beta^{\mathrm{p}}$ is set equal to zero if the pressure is negative. The elastic parameters λ_{i} and $\mu_{\mathrm{i}}(i=\alpha,\beta)$ are given by

$$\begin{aligned} \lambda_i &= \frac{E_i(1+\nu_i)}{2} \\ \mu_i &= \frac{E_i}{2(1+\nu_i)} \end{aligned} \tag{16}$$

Here, E_{i} is Young's modulus for phase i. We adopt Mulliken and Boyce (2006) assumption that Poisson's ratio has a constant value of 0.38 and 0.35 for the PC and the PMMA, respectively. Young's modulus, E, of the material which is the sum of Young's moduli of the individual phases, is assumed to be equal to the storage modulus measured during DMA tests for the material. The computation of Young's modulus for individual phases from the storage modulus is described in (Mulliken and Boyce, 2006). We note that E depends upon the reference temperature and the nominal strain rate. The values of E_α and E_β as a function of the temperature and the strain rate are not listed since they are derived from functions given as MATLAB routines in Appendices C and D of Mulliken's thesis. (Mulliken, 2004) which were converted to FORTAN 90 subroutines. Typical values of E_α and E_β at 300 K and nominal strain rate of 5,000/s equal, respectively, 1.678 GPa and 0.345 GPa for the PC; while for the PMMA they are 2.894 GPa and 1.943 GPa. The variation of E_α and E_β with temperature at low strain rates for the PC and the PMMA are, respectively, depicted in Figs. 5 and 6 in (Mulliken and Boyce, 2006).

We note that the value of $\dot{\gamma}_{0\alpha}^{\mathrm{p}}$ in Eq. $(14)_1$ for the PMMA is of the order of 10^{219} but that of $\dot{\gamma}_{0\beta}^{\mathrm{p}}$ is 10^3. Thus $\dot{\gamma}_\alpha^{\mathrm{e}}$ can potentially be very

Table 1
Values of material parameters for the PC and the PMMA (Mulliken and Boyce, 2006); see the text following Eq. (16) for values of E.

	PC			PMMA		
	α	β	B	α	β	B
ν	0.38	0.38		0.35	0.35	
$\dot{\gamma}_0^{\mathrm{p}}(\mathrm{s}^{-1})$	2.94×10^{16}	3.39×10^{5}		6.95×10^{219}	1.77×10^{3}	
ΔG (J)	3.744×10^{-18}	3.769×10^{-20}		5.528×10^{-18}	6.036×10^{-20}	
α_p	0.168	0.245		0.26	0.26	
h_α (MPa)	250	N/A		200	N/A	
s_α^{ss}(MPa)	$0.67s_\alpha^0$	N/A		$0.73s_\alpha^0$	N/A	
C_R(MPa) (at 300 K)			14.2			14.0
N_l			5.29			4.84

large as compared to $\dot{\gamma}^{p}_{\beta}$ for the PMMA. However, for the PC, $\dot{\gamma}^{p}_{0\alpha}$ and $\dot{\gamma}^{p}_{0\beta}$ are of the order of 10^{16} and 10^{5} respectively.

5. Verification of the user defined subroutine

In order to establish the range of validity of the Mulliken–Boyce constitutive relations, we conduct numerical simulations in which equations expressing the conservation of mass, the conservation of linear momentum, the conservation of moment of momentum, and the constitutive equations subject to initial and boundary conditions pertinent to the test configuration are solved numerically by the Finite Element Method (FEM). The initial-boundary-value problem is solved using the commercial Finite Element (FE) software, LSDYNA, where the constitutive equations are implemented as a user defined subroutine. We used 8-node brick elements with one-point integration rule and a lumped mass matrix derived from the consistent mass matrix by the row sum technique. Hence, the material is assumed to be homogeneous in each element. Equations of motion are integrated with an explicit conditionally stable algorithm and the time step size is taken as a fraction of that required for the elastic dilatational wave to propagate through the smallest element in the mesh. Also, deformations are assumed to be locally adiabatic. The unknowns at a node are $\mathbf{x}, \mathbf{v}, \mathbf{F}^{p}_{\alpha}, \mathbf{F}^{p}_{\beta}, s_{\alpha}, \theta$, and the mass density ρ. For a 3D problem the number of unknowns at a node equals 27. Verification of the user defined subroutine for isothermal deformations is described below.

5.1. Verification of the user defined subroutine during elastic deformations

For finite simple extensional and simple shear homogeneous deformations of an elastic body, Batra (2001) gave analytical expressions for stresses with the material modeled by four different constitutive equations. The constitutive equations $(10)_1$ and $(10)_2$ for elastic deformations of phases α and β correspond to Eq. (4) in (Batra, 2001). We perform numerical simulations using LSDYNA of simple extension and simple shear deformations of one FE considering only phase α. Plastic deformations and strain softening effects are ignored. The resulting stress vs. strain curves are converted to normalized stress/load vs. strain/stretch measures as described in (Batra, 2001) and compared with those obtained from the analytical expressions in Fig. 9. It can be seen that the normalized stress vs. strain curves from the numerical simulations compare well with the analytical results. Similar tests were also performed by considering only phase β. Note that the deformation is homogeneous during these tests.

To verify the user defined subroutine during inhomogeneous deformations we study deformations of a square plate with a through-the-thickness circular void centered at the plate centroid. The schematic diagram of the problem is depicted in Fig. 10. Dimensions of the plate and the circular void are: $L = 1$ mm, $h = 0.04$ mm, and $a = 0.04$ mm. The plate is deformed by pulling axially its top and bottom surfaces with a speed that increases from zero to a steady value, v_0, in time $t^0 = 1.0\ \mu$s. The nominal axial strain rate, v_0/L, was chosen to be 5000/s.

In the referential description of motion balance laws governing deformations of the plate material are:

$$\text{linear momentum}: \quad \rho_0 \dot{\mathbf{v}} = \nabla \cdot \widehat{\mathbf{T}} \text{ in } \Omega \tag{17}$$

$$\text{moment of momentum}: \quad \widehat{\mathbf{T}}\mathbf{F} = \mathbf{F}^{T}\widehat{\mathbf{T}}^{T} \text{ in } \Omega \tag{18}$$

Here ρ_0 is the mass density in the reference configuration, $\mathbf{F}$ the deformation gradient, $\mathbf{v}$ the velocity field defined as $\mathbf{v} = \dot{\mathbf{x}}$, and a superimposed dot denotes the material time derivative defined as $\frac{\partial}{\partial t}|_{X_i=\text{Constant}}$ in the Lagrangian description of motion, and as $\frac{\partial}{\partial t} + \frac{\partial x_l}{\partial t}\frac{\partial}{\partial x_l}$ in the Eulerian description of motion. Furthermore, $\widehat{\mathbf{T}}$ is the first Piola-Kirchhoff stress tensor, and $\nabla \cdot \widehat{\mathbf{T}}$ the divergence of $\widehat{\mathbf{T}}$ with respect to coordinates in the reference configuration.

Because of the symmetry of the plate geometry, the void, and of the initial and the boundary conditions about the three centroidal planes, we assume that plate's deformations are symmetric about the X_1, the X_2, and the X_3 axes shown in Fig. 10. Accordingly, deformations of one-eighth of the plate in Fig. 10 (shown in grey) are analyzed under the following boundary conditions.

$$x_1 = 0 \quad \bar{t}_2 = 0 \quad \bar{t}_3 = 0 \quad \text{on} \quad X_1 = 0 \tag{19a}$$

$$\bar{t}_1 = 0 \quad \bar{t}_2 = 0 \quad \bar{t}_3 = 0 \quad \text{on} \quad X_1 = L \tag{19b}$$

$$x_2 = 0 \quad \bar{t}_1 = 0 \quad \bar{t}_3 = 0 \quad \text{on} \quad X_2 = 0 \tag{19c}$$

$$x_3 = 0 \quad \bar{t}_1 = 0 \quad \bar{t}_2 = 0 \quad \text{on} \quad X_3 = 0 \tag{19d}$$

$$\bar{t}_1 = 0 \quad \bar{t}_2 = 0 \quad \bar{t}_3 = 0 \quad \text{on} \quad X_3 = h/2 \tag{19e}$$

$$v_2 = \begin{cases} v_0 \frac{t}{t^0}, & 0 \le t < t^0 \\ v_0, & t \ge t^0 \end{cases} \quad \bar{t}_1 = 0 \quad \bar{t}_3 = 0 \quad \text{on} \quad X_2 = L \tag{19f}$$

$$\widehat{T}_{i\beta} N_\beta = 0 \quad (i = 1,2,3; \beta = 1,2) \quad \text{on} \quad (X_1)^2 + (X_2)^2 = a^2 \tag{19g}$$

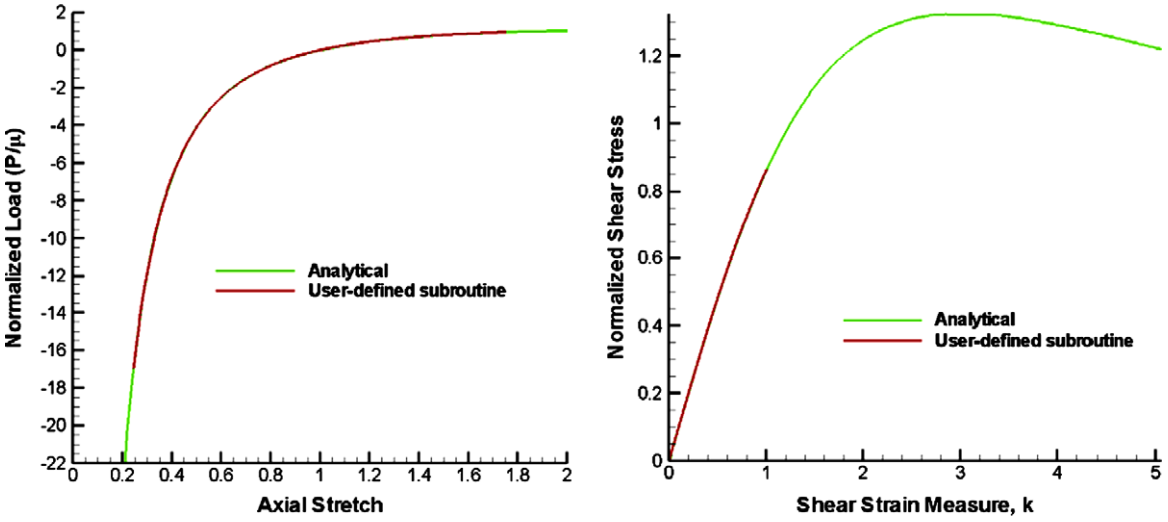

Fig. 9. Comparison of the normalized load vs. the axial stretch curves from numerical simulations of simple extension and the analytical expressions (left), and normalized shear stress vs. shear strain measure from numerical simulations of simple shear and the analytical expressions (right).

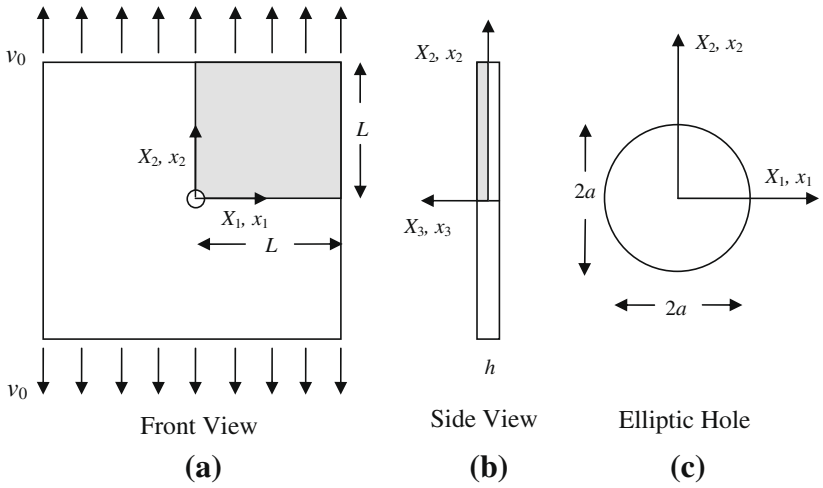

Fig. 10. (a) Front and (b) side views of a square plate with a through-the-thickness hole; (c) the shape of the circular hole.

Here $\bar{\mathbf{t}}$ is the traction vector in the deformed configuration, **N** is an outward unit normal to the surface of the elliptic void in the reference configuration, and **X** and **x** are position vectors of the same material point in the undeformed and the deformed configurations, respectively.

Initially the plate is assumed to be at rest and in a stress-free state.

The test is performed using two material subroutines: (1) the inbuilt material subroutine in LSDYNA for elastic materials, MAT_ELASTIC, and (2) the user defined subroutine for glassy polymers. For the test, only phase α is considered and plastic deformations and strain softening effects are ignored. The values of Young's modulus and Poisson's ratio were 1.678 GPa and 0.38, respectively. Values of the material parameters correspond to their values for PC at nominal strain rate of 5000/s and temperature of 300 K.

The spatial distributions of the 22-component of the true strain tensor from the two tests at $t = 7\mu s$ are compared in Fig. 11. The contour plots of the variable found by using the inbuilt subroutine is shown in the Figure on the left and the percentage difference in the variable using the two material subroutines is depicted in the Figure on the right. It can be seen that the maximum value of the 22-component of the true strain tensor has reached 8% and that the percentage difference is close to zero within a majority of the domain. The maximum percentage difference in the variable from the user defined subroutine is only 1.5%. While the constitutive equations in the inbuilt subroutine for elastic materials are not the same as those given in Eq. (10), the results from the two tests should be close to each other as long as the deformations are small (strains are less than 10%).

5.2. Verification of the user defined subroutine for strain softening variable

Strain softening in the glassy polymer is reproduced by the evolution of the softening variable s_α given by Eq. (15). During uniaxial deformations, the effective plastic strain rate jumps at yield to a value of $\sqrt{3/2}\dot{\varepsilon}$, where $\dot{\varepsilon}$ is the nominal axial strain rate and remains more or less constant after yield. The factor $\sqrt{3/2}$ follows from computing the strain rate tensor for isochoric axial deformation and Eq. (7). The evolution of s_α can be estimated by integrating Eq. (15) with the effective plastic strain rate in phase α assumed to be equal to 6.12×10^3/s, which corresponds to an applied axial strain rate of 5000/s. During integration the effective plastic strain rate is assumed to be non-zero only after $t = 13\ \mu s$ (cf. Appendix A), because the deformation is essentially elastic prior to that time. The time history plots of s_α calculated using the approximate solution, and that obtained during a simulation of the uniaxial compression test at 5000/s using the user defined subroutine in LSDYNA are shown in Fig. 12. It can be seen that the evolution of s_α computed using the approximate solution is reasonably close to the results obtained using the user defined subroutine. The difference in the results arises because the effective plastic strain rate in phase α during a uniaxial compression test is not constant after σ_{mag} has reached the maximum.

5.3. Verification of user defined subroutine for phase B

The Cauchy stress in phase B, given by Eq. (11), depends only upon the deformation gradient. Hence, the Cauchy stress in phase B during uniaxial compression can be estimated by assuming that the deformation is isochoric. This is a reasonable assumption since plastic deformations of phases α and β have been assumed to be isochoric and elastic deformations are small compared to plastic deformations at strains greater than 0.2. To validate the assumption the total axial stretch is compared to the plastic axial stretch in phase α during a uniaxial compression test in Fig. 13. It can be seen that the plastic axial stretch is close to the total axial stretch.

Hence, the deformation gradient can be assumed to be given by

$$\mathbf{F} = \begin{bmatrix} \lambda^{-1/2} & 0 & 0 \\ 0 & \lambda^{-1/2} & 0 \\ 0 & 0 & \lambda \end{bmatrix} \tag{20}$$

Here λ is the stretch during uniaxial extension and the true axial strain is given by $|\ln\lambda|$. The true axial stress in phase B, $\sigma^{\text{B}}_{\text{approx}}$, can be approximated by

$$\sigma^{\text{B}}_{\text{approx}} = \frac{C_R}{3}\sqrt{\frac{3N_l}{(\lambda^2+2/\lambda)}}L^{-1}\left(\sqrt{\frac{(\lambda^2+2/\lambda)}{3N_l}}\right)\frac{2}{3}\left(\lambda^2-\frac{1}{\lambda}\right) \tag{21}$$

The true axial stress in phase B during a uniaxial compression test is compared in Fig. 14 with that given by Eq. (21). It is clear that the two sets of values are very close to each other.

5.3.1. Comparison of predictions from constitutive relations with experimental results

The true axial stress vs. the true axial strain curves for the PC and the PMMA computed using the user defined subroutine in LSDYNA and the material parameters reported in (Mulliken and Boyce, 2006) did not match well with the results from simulations

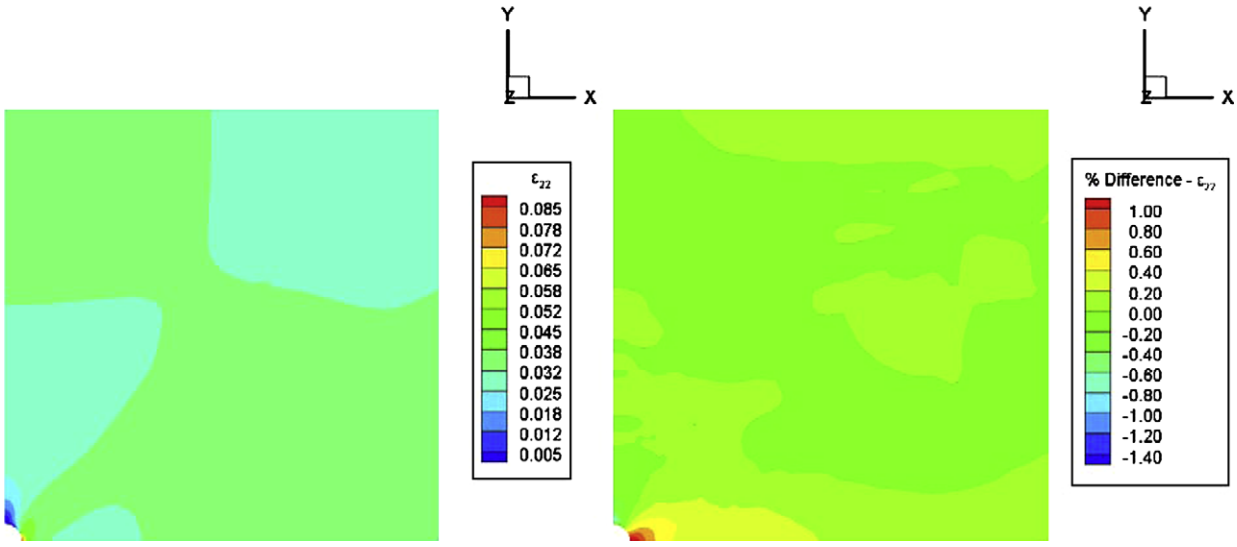

Fig. 11. Comparison of the 22-component of the true strain tensor at $t = 7$ μs from an inbuilt subroutine for elastic materials and from the user defined subroutine for glassy polymers. Only phase α is considered, and plastic deformations and strain softening are ignored in the user defined subroutine.

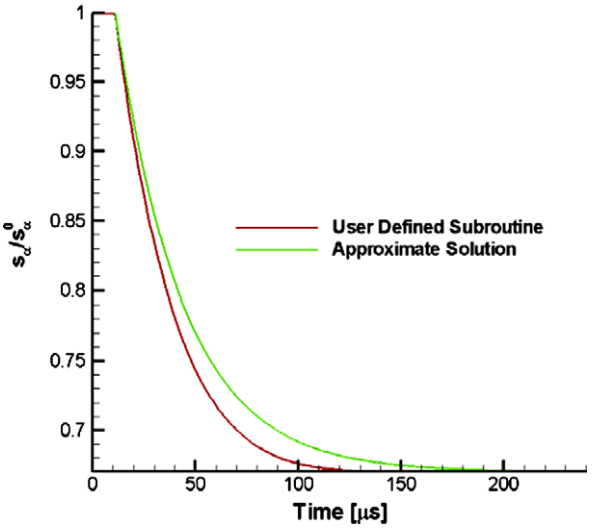

Fig. 12. Time history plots of the softening variable s_α computed using an approximate solution and that obtained by simulating the uniaxial compression test using the user defined subroutine in LSDYNA.

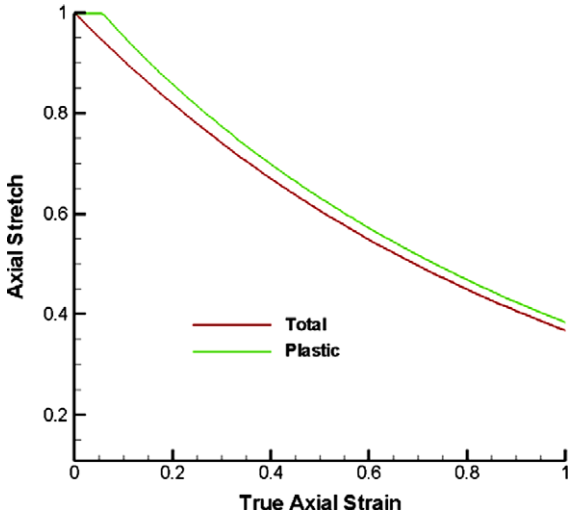

Fig. 13. Comparison of the total axial stretch and the plastic stretch in phase α during a simulation of the uniaxial compression test on the PC.

by Mulliken and Boyce in the post-yield region. However, we were able to find modified values of s_α^{ss} and h_α for the PMMA, and of s_α^{ss}, h_α, and N_l for the PC, listed in Table 2, that replicated well the results of simulations by Mulliken and Boyce.

The experimental true axial stress vs. the true axial strain curves for uniaxial compressive deformations of the PC are compared in Fig. 15 with those from numerical simulations by Mulliken and Boyce (2006) using material parameters in Table 1 and using the user defined subroutine in LSDYNA with the material parameters from Table 2. It can be seen that the predicted results match well with the test data at all strain rates.

For the PMMA, the experimental true axial stress vs. true axial strain curves for uniaxial compressive deformations are compared in Fig. 16 with those obtained from numerical simulations by Mulliken and Boyce (2006) using material parameters in Table 1 and using the user defined subroutine in LSDYNA with the material parameters from Table 2. It is clear that the predicted results match well with the test data at low strain rates but not at medium and high strain rates. The softening following the peak in the stress–strain curve observed experimentally is not exhibited by results of numerical simulations. Simulations with the user defined subroutine were not performed at strain rates less than 0.001/s because of the high computational time involved.

6. Modified constitutive equations

As noted above, Mulliken and Boyce's constitutive equations predict well the viscoelastic response and the yielding of the PC and the PMMA at all strain rates. However, they do not predict well the experimentally observed response of the PMMA at medium and high strain rates in the post-yield region. It has been reported in the literature (Rittel, 1999; Leonov and Prokunin, 1994; Moy et al., 2003a) that the temperature of glassy polymers increases during moderate and high strain rate deformations. Arruda et al. (1995) observed a temperature rise of 20 K in PMMA disks tested in compression, while Garg et al. (2008) reported a temperature rise of 40 K in PC samples during high strain rate uniaxial compres-

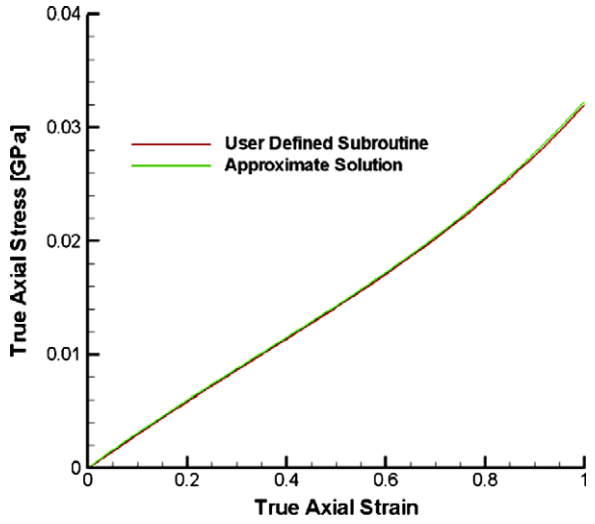

Fig. 14. Comparison of the true axial stress in phase B during a simulation of the uniaxial compression test with the approximate solution given by Eq. (21).

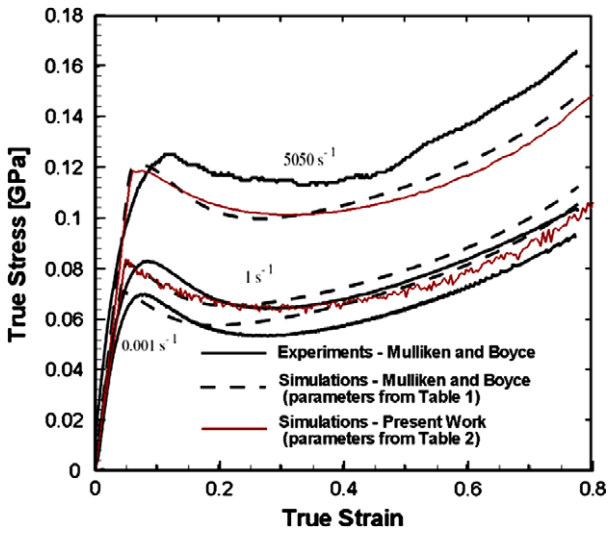

Fig. 15. True axial stress vs. true axial strain curves for the PC in uniaxial compression at different axial nominal strain rates. (*Source*: Mulliken and Boyce (2006).)

sion tests. Mulliken and Boyce's simulations of uniaxial compression tests considered isothermal deformations of the PC and the PMMA. Hence, we first consider the temperature rise due to plastic working being converted to heating during high strain rate deformations of glassy polymers.

6.1. Modification of constitutive equations for temperature rise

We assume that all of the energy dissipated due to plastic working is converted into heating. The conservation of internal energy with heat conduction neglected (i.e., locally adiabatic deformations) can be written as

$$\rho c\dot{\theta} = \mathrm{tr}\left(\boldsymbol{\sigma}_\alpha \widetilde{\mathbf{D}}^{\mathrm{p}}_\alpha\right) + \mathrm{tr}\left(\boldsymbol{\sigma}_\beta \widetilde{\mathbf{D}}^{\mathrm{p}}_\beta\right) \tag{22}$$

where c is the specific heat and θ the temperature. Thus the temperature rise at every point of the body can be computed.

The elastic parameters λ_i and μ_i in Eq. (10), the rubbery modulus C_R for phase B, and the effective plastic strain rates given by Eq. (14) are assumed to depend upon the current value of the temperature rather than upon the temperature in the reference configuration. We first compare computed results with test findings for a PC and then for a PMMA. We use Garg et al. (2008) test data for compressive deformations of PC at high strain rates. They measured the temperature using an infrared detector system. The true axial stress vs. the true axial strain curve reported by Garg et al. did not agree well with that predicted by using the material parameters for the PC given in Table 2 and the Mulliken and Boyce constitutive equations. The material parameters for the PC tested by Garg et al. were identified such that the true axial stress vs. the true axial strain curve from numerical simulations compared well with their experimental results. Values of parameters that are different from those given in Table 2 for the PC are listed in Table 3. The tem-

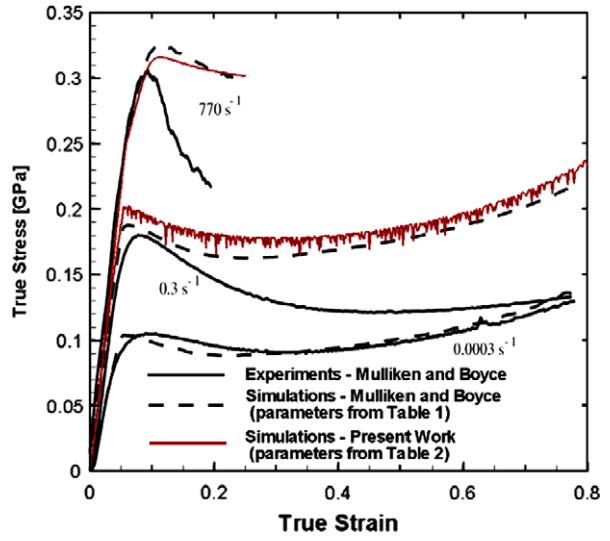

Fig. 16. True axial stress vs. true axial strain curves for the PMMA in uniaxial compression at different axial nominal strain rates.

Table 2
Value of material parameters for the PC and the PMMA used in the user defined subroutine; see the text following Eq. (16) for values of E.

	PC			PMMA		
	α	β	B	α	β	B
ν	0.38	0.38		0.35	0.35	
$\dot{\gamma}^{\mathrm{p}}_0(\mathrm{s}^{-1})$	2.94×10^{16}	3.39×10^{5}		6.95×10^{219}	1.77×10^{3}	
ΔG (J)	3.744×10^{-18}	3.769×10^{-20}		5.528×10^{-18}	6.036×10^{-20}	
α_{p}	0.168	0.245		0.26	0.26	
h_α (MPa)	125	N/A		200	N/A	
s^{ss}_α(MPa)	$0.42s^0_\alpha$	N/A		$0.50s^0_\alpha$	N/A	
C_R(MPa) (at 300 K)			14.2			14.0
N_l			2.25			2.2

Table 3
Values of the material parameters for the PC tested by Garg et al. (2008) that are different from the PC tested by Mulliken and Boyce.

Material parameter	Value
h_α (MPa)	150
s_α^{ss}(MPa)	$0.50 s_\alpha^0$
N_l	1.96

perature rise was then computed using Eq. (22) and compared with the experimental findings of Garg et al. in Fig. 17. Values of the mass density and the specific heat taken from the literature are listed in Table 4. It is clear that there is a close agreement between the computed and the test results.

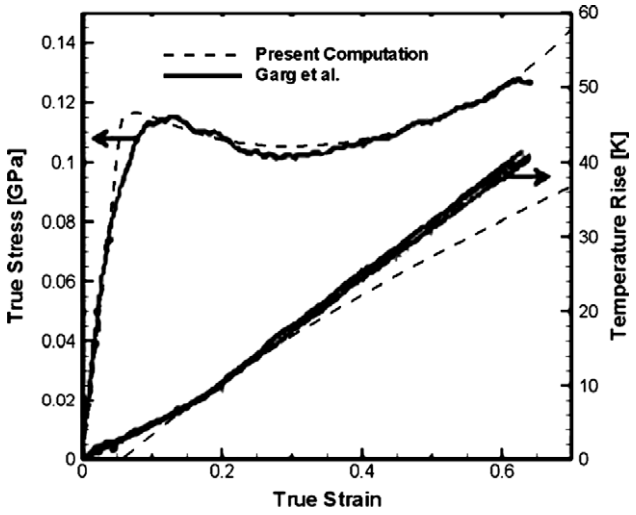

Fig. 17. Comparison of the two true axial stress vs. the true axial strain curves, and the two temperature rise vs. the true axial strain curves during uniaxial compression of the PC at a nominal axial strain rate of 3400/s. (*Source*: Garg et al. (2008).)

Table 4
Values of the mass density and the specific heat of PC and PMMA.

Material property	PC	PMMA
ρ (g/cm^3)	1.20	1.14
c (J/(gK))	1.20	1.46

The true axial stress vs. the true axial strain curves for the PC and the PMMA tested by Mulliken and Boyce (2006) with material parameters listed in Table 2 are recomputed, with and without considering the heat produced due to plastic work, and compared with the corresponding experimental results in Fig. 18. It can be seen that the material has softened more with the consideration of heating due to plastic working, but the predicted stress–strain curves do not emulate well the experimental ones for moderate and high strain rate deformations.

6.2. Modification of constitutive equations for plastic strain rates

In the Mulliken and Boyce constitutive equations strain softening is captured by the softening variable, s_α, whose initial value equals $0.077\mu_\alpha/(1-\nu_\alpha)$ and depends only on the initial values of the applied strain rate and the temperature. The evolution of s_α is given by Eq. (15) and depends on its current value and the effective plastic strain rate. During isothermal deformations at constant strain rate deformations studied by Mulliken and Boyce, the value of $0.077\mu_\alpha/(1-\nu_\alpha)$ does not change. However, during generalized deformations of glassy polymers the value of $0.077\mu_\alpha/(1-\nu_\alpha)$ may change. Hence, we separate the variable s_α in the Mulliken and Boyce constitutive equations into two variables t_α and $\hat{s}_\alpha$ whose meanings are as follows: (1) variable $\hat{s}_\alpha = 0.077\mu_\alpha/(1-\nu_\alpha)$ depends on the current value of the temperature and the strain rate, and (2) a new variable t_α that simulates the evolution of the strain softening variable s_α in the Mulliken and Boyce constitutive equations.

Constitutive relations $(14)_1$ and (15) for the effective plastic strain rate and the strain softening parameter for phase α are modified to the following equations.

$$\dot{\gamma}_\alpha^p = \dot{\gamma}_{0\alpha}^p \exp\left[-\frac{\Delta G_\alpha}{k\theta}\left(1-\frac{\tau_\alpha}{t_\alpha \hat{s}_\alpha + \alpha_\alpha^p p}\right)\right] \tag{23}$$

$$\dot{t}_\alpha = \frac{h_\alpha}{\hat{s}_\alpha^0}\left(1-\frac{t_\alpha}{t_\alpha^{ss}}\right)\dot{\gamma}_\alpha^p \tag{24}$$

$$\hat{s}_\alpha = \frac{0.077\mu_\alpha}{1-\nu_\alpha} \tag{25}$$

Here t_α is an internal variable, t_α^{ss} is a material parameter, and $\hat{s}_\alpha^0$ is the reference value of $\hat{s}_\alpha$. In Eq. (23), a new internal variable t_α is

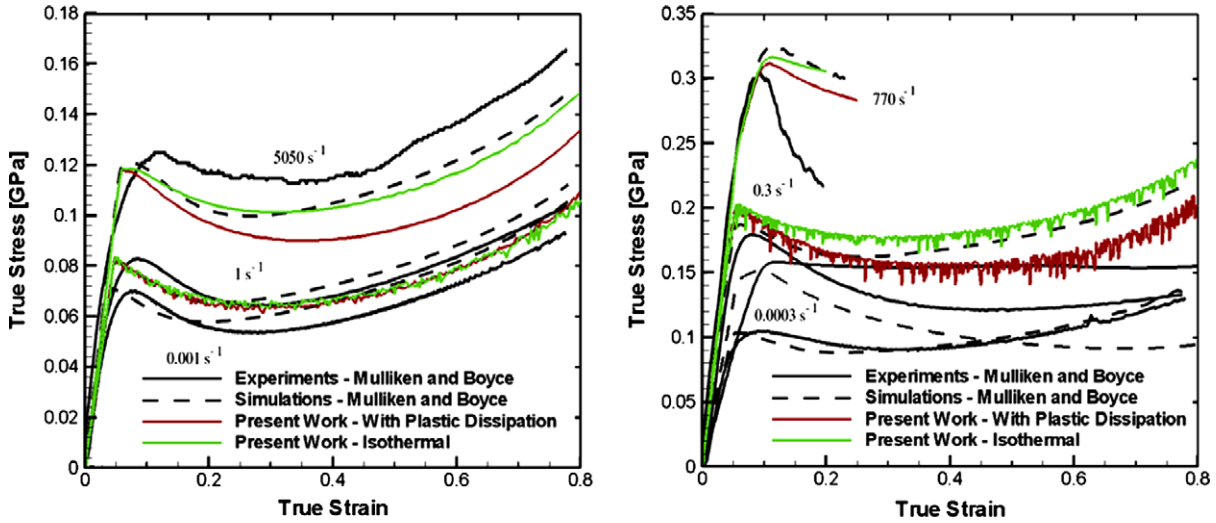

Fig. 18. Comparison of the true stress vs. the true strain curves of the PC (left) and the PMMA (right) in uniaxial compression computed using Mulliken and Boyce's constitutive equations with and without consideration of the temperature rise due to plastic dissipation.

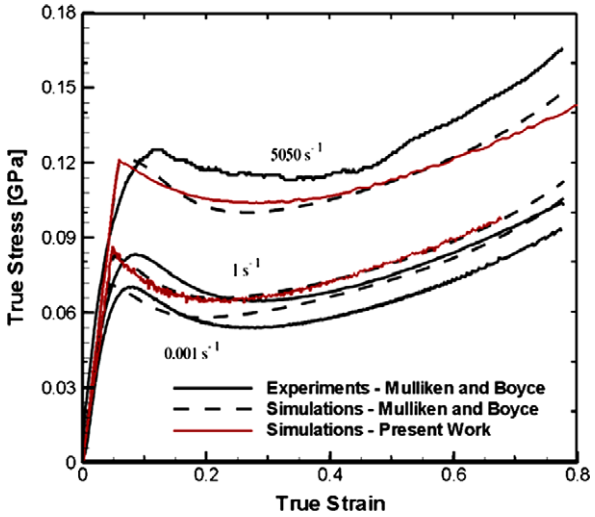

Fig. 19. Comparison of the true axial stress vs. the true axial strain curves of the PC deformed in uniaxial compression obtained using experimental data, constitutive equations proposed by Mulliken and Boyce, and the modified constitutive equations.

introduced that evolves according to Eq. (24) during plastic deformations; its rate of evolution is proportional to $\dot{\gamma}_\alpha^p$ and equals zero when either deformations are elastic or when t_α is close to t_α^{ss}. The strain softening in glassy polymers at low strain rates and high temperatures is captured by the evolution of t_α from an initial value of 1.0 to t_α^{ss}. The parameter t_α^{ss} is determined by the ratio of the local minima in the axial stress after yielding to the axial stress at yielding. The variable $\hat{s}_\alpha$ is given by Eq. (25) but with μ_α depending upon the present temperature and the current effective strain rate. Hence, the evolution of $\hat{s}_\alpha$ simulates thermal softening as the temperature at a material point evolves. The parameter $\hat{s}_\alpha^0$ in Eq. (24) is a fraction of the reference value of the shear modulus. Similar to Eqs. (23) and (24), the constitutive equation $(14)_2$ for phase β is modified to the following equations:

$$\dot{\gamma}_\beta^p = \dot{\gamma}_{0\beta}^p \exp\left[-\frac{\Delta G_\beta}{k\theta}\left(1-\frac{\tau_\beta}{t_\beta \hat{s}_\beta + \alpha_\beta^p p}\right)\right] \tag{26}$$

$$\dot{t}_\beta = \frac{h_\beta}{\hat{s}_\beta^0}\left(1-\frac{t_\beta}{t_\beta^{ss}}\right)\dot{\gamma}_\beta^p \tag{27}$$

$$\hat{s}_\beta = \frac{0.077\mu_\beta}{1-\nu_\beta} \tag{28}$$

where variables have meanings similar to those for phase α. The determination of the new material parameters t_α^{ss} and t_β^{ss} is described in Appendix A.

The simulation of simple tensile deformations of a body comprised of phase α revealed that a change in the value of the internal variable t_α from 0.9 to 0.6 increased the effective plastic strain rate by an unrealistic 13 orders of magnitude. Accordingly, Eqs. (23) and (26) are modified to

$$\dot{\gamma}_i^p = \min\left(\dot{\gamma}_{0i}^p \exp\left[-\frac{\Delta G}{k\theta}\left(1-\frac{\tau_i}{t_i\hat{s}_i+\alpha_i^p p}\right)\right],\ 10^5/s\right), \quad i=\alpha,\beta \tag{29}$$

that limits the maximum effective plastic strain rate in phases α and β to 100,000/s.

The temperature rise due to plastic dissipation is not considered when the nominal strain rate is less than 0.001/s or the deformations are quasi-static.

Material parameters for the PC and the PMMA tested by Mulliken and Boyce are given in Table 5.

7. Validation of the modified constitutive relations

The true axial stress vs. the true axial strain curves for the PC and the PMMA tested in uniaxial compression computed using the modified constitutive Eqs. (23)–(28) and values of material parameters listed in Table 5 are compared with the experimental and the numerical results of Mulliken and Boyce in Figs. 19 and 20. The PC and the PMMA are assumed to be initially at a temper-

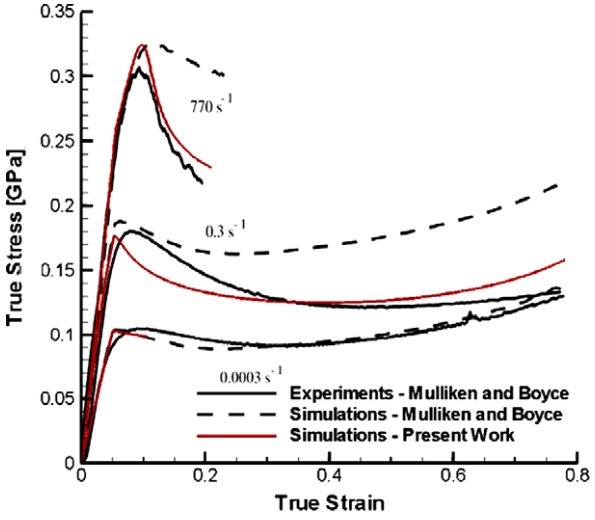

Fig. 20. Comparison of the true axial stress vs. the true axial strain curves of the PMMA deformed in uniaxial compression obtained using experimental data, constitutive equations proposed by Mulliken and Boyce, and the modified constitutive equations.

Table 5
Values of material parameters for the modified constitutive equations for the PC and the PMMA; see the text following Eq. (16) for values of E.

	PC			PMMA		
	Phase α	Phase β	Phase B	Phase α	Phase β	Phase B
ν_i	0.38	0.38		0.35	0.35	
$\dot{\gamma}_{0i}^p(/s)$	2.94×10^{16}	3.39×10^{5}		6.95×10^{219}	1.77×10^{3}	
ΔG_i(J)	3.744×10^{-18}	3.769×10^{-20}		5.528×10^{-18}	6.036×10^{-20}	
α_i^p	0.168	0.245		0.26	0.26	
h_i (MPa)	125	400		200	500	
t_i^{ss}	0.33	2.00		0.73	0.45	
C_R at 300 K (MPa)			35.0			14.0
N_l			12.25			2.1
c (J/(gK))	1.20			1.46		
ρ (kg/m^3)	1.20			1.14		

ature of 300 K. It can be seen that the modified constitutive equations predict well the experimental results in the post-yield region at moderate and high strain rates.

The modified constitutive equations were also used to predict the true axial stress vs. the true axial strain curves for the PC and the PMMA studied by Richeton et al. (2007). The value of Young's modulus used by Richeton et al. was different from that given by Mulliken and Boyce. Hence, in our computations, values of Young's modulus for the α and the β phases were multiplied by a factor such that their sum nearly equaled the value of Young's modulus used by Richeton et al. For other material parameters the values listed in Table 5 are used. It can be seen from results evidenced in Fig. 21 that the modified constitutive equations predict well the yield and the post-yield response of the PC and the PMMA at high strain rates. The results in Fig. 21 correspond to uniaxial compression tests conducted at 298 K and the nominal axial strain rate of 2,202/s and 2,265/s, respectively, for the PC and the PMMA. The variation of Young's modulus with strain rate and temperature for the PC and the PMMA tested by Richeton et al. and Mulliken and Boyce are compared in Fig. 3.27 of (Varghese, 2008).

7.1. Other loading conditions

The mechanical response of glassy polymers depends on the state of stress. Fig. 22 exhibits the magnitude of the Cauchy stress vs. the magnitude of the true strain tensor curves for a PC and a PMMA deformed in uniaxial compression, tension, and simple shear. The pressure coefficients for phases α and β cause the yield stress to depend on the hydrostatic pressure at a material point as is evident from the form of the constitutive Eqs. (23) and (26) for the effective plastic strain rate. Thus the stress–strain curves for uniaxial tensile and compressive deformations are different.

The plots of σ_{mag} vs. ε_{mag} with the pressure coefficients taken as zero are shown in Fig. 23. The yield stress in this case did not change with the stress state for uniaxial compression and tension. However, the stress vs. strain plots showed a difference during

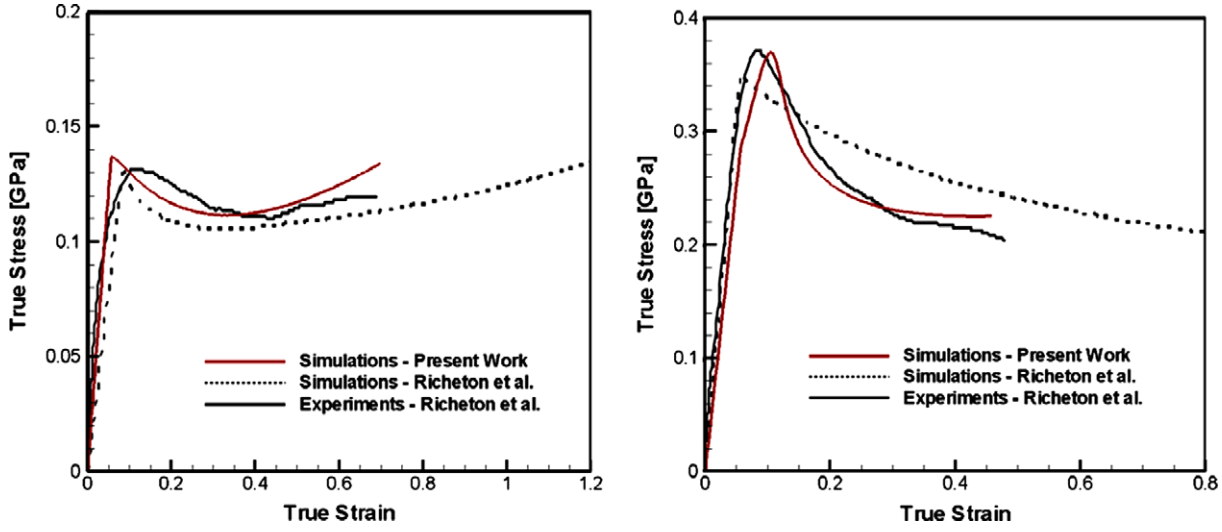

Fig. 21. Comparison of the true axial stress vs. the true axial strain curves of the PC (left) and the PMMA (right) in uniaxial compression obtained using experimental data, constitutive equations proposed by Richeton et al., and the modified constitutive equations.

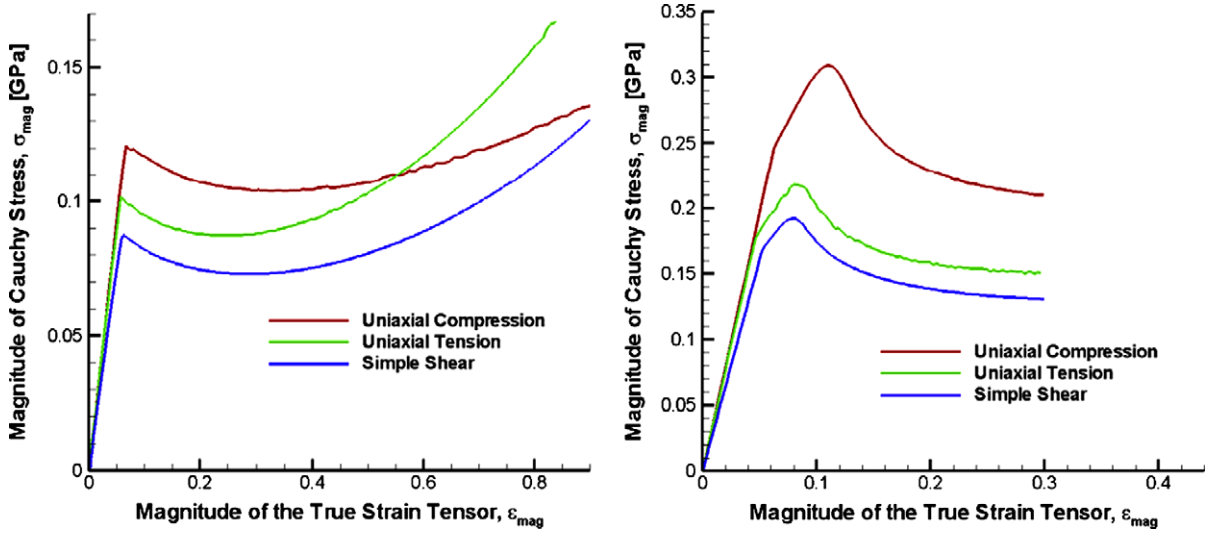

Fig. 22. The magnitude of the Cauchy stress tensor vs. the magnitude of the true strain tensor for a PC (left) and a PMMA (right) at nominal strain rates of 5050/s and 770/s, respectively, in uniaxial compression, uniaxial tension, and simple shear deformations.

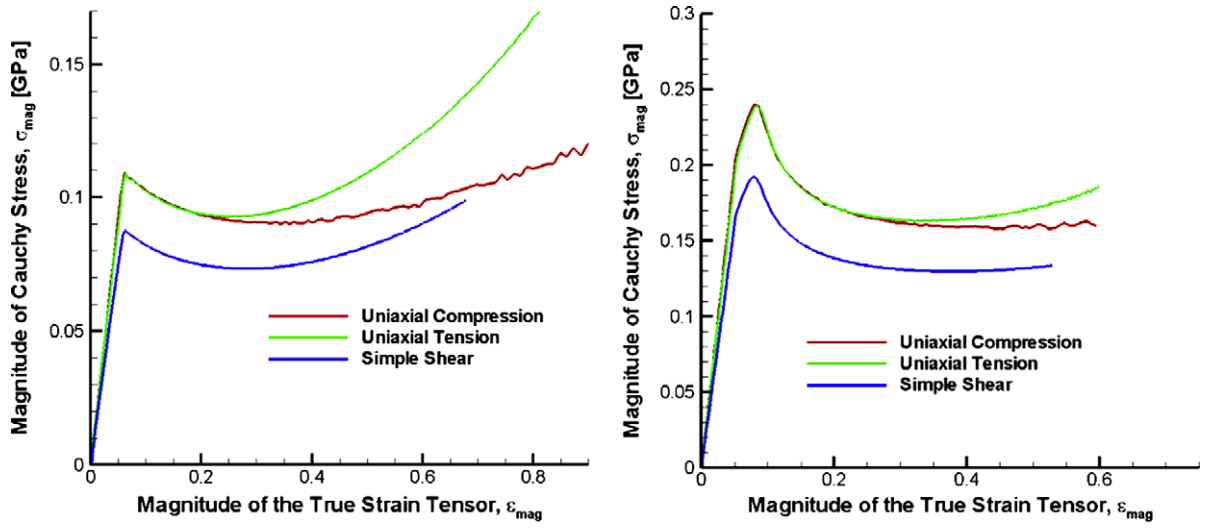

Fig. 23. The magnitude of the Cauchy stress tensor vs. the magnitude of the true strain tensor for a PC (left) and a PMMA (right) at nominal strain rates of 5050/s and 770/s, respectively, in uniaxial compression, uniaxial tension, and simple shear deformations with the pressure coefficients taken as zero.

strain hardening under different stress states. This is because the value of the variable λ^p in Eq. (11) is different in uniaxial compression and tension for the same value of the true axial strain.

8. Temperature rise during compressive loading

It is interesting to delineate contributions from deformations of individual phases to the temperature rise. Fig. 24 shows the temperature rise in different phases of a PC deformed in uniaxial compression at nominal axial strain rates of 5050/s and 1/s. It can be seen that at the strain rate of 1/s, only phase α contributes to the temperature rise; however, at the strain rate of 5050/s, deformations of the β phase generate more heat than that at a strain rate of 1/s.

Results of similar numerical tests on a PMMA are shown in Fig. 25 at strain rates of 770/s and 0.3/s. In PMMA, at the strain rate of 770/s, both phases α and β contribute equally to the temperature rise; however, at the strain rate of 0.3/s, the heat generated due to deformations of the α phase exceeded that due to deformations of the β phase.

9. Remarks

In previous works (e.g., see Batra and Adam (1991), Batra and Jayachandran (1992), and Batra and Chen (2001)) we have used various thermo-visco-elasto-plastic relations to study high strain rate deformations of metals. A major difference between the deformations of metals and glassy polymers is that the former generally do not exhibit strain hardening following the strain softening. The plastic straining of metals elevates their temperatures and strain hardens them. When the softening due to temperature rise exceeds hardening due to plastic working, the material exhibits strain softening. The strain softening of polymers is possibly due to either the breaking or the rearrangement of molecular chains. The stretching of molecular chains is believed to induce strain hardening in polymers.

10. Conclusions

Mulliken and Boyce's constitutive equations for glassy polymers have been modified to better correlate predictions from them with

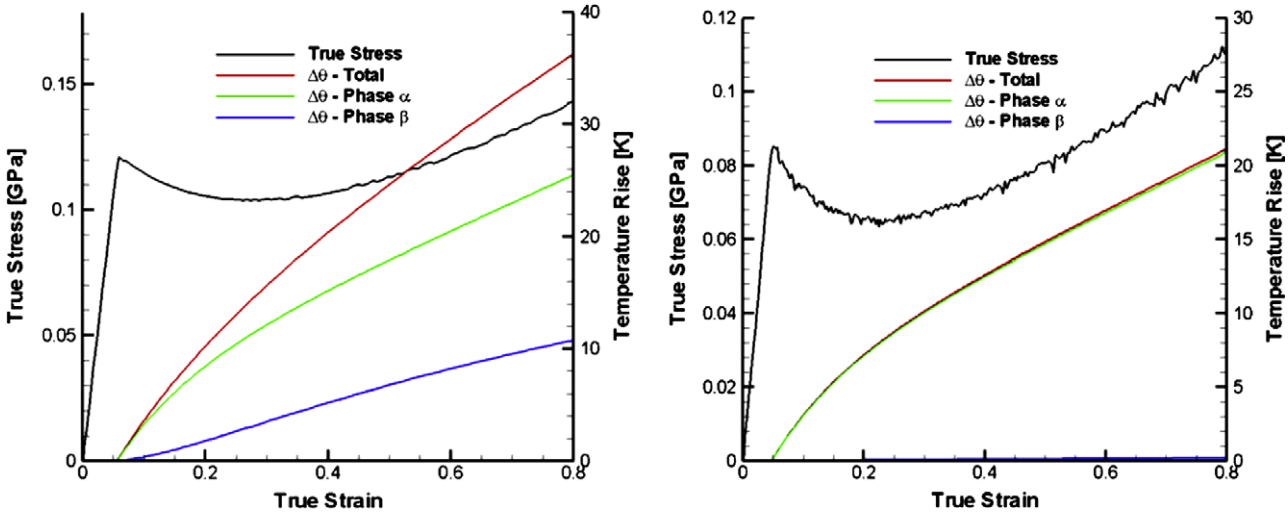

Fig. 24. Comparison of the temperature rise in phases α and β during uniaxial compressive deformations of a PC at strain rates of 5050/s (left) and 1.0/s (right).

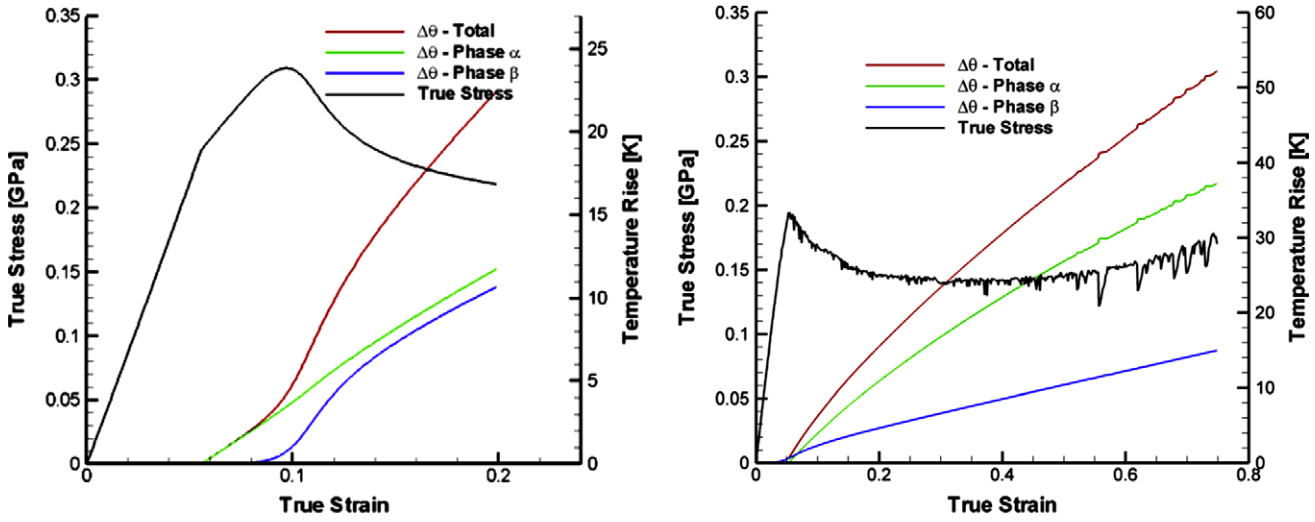

Fig. 25. Comparison of the temperature rise in phases α and β during uniaxial compressive deformations of a PMMA at strain rates of 770/s (left) and 0.3/s (right).

experimental results at high strain rates. Values of newly introduced parameters have been determined, and it has been shown that the response predicted from the modified constitutive equations matches well with experimental results reported in two independent studies. The constitutive equations predict well the viscoelastic, yielding, and post-yielding behavior of PMMA and PC in uniaxial compression at all strain rates.

Two internal variables t_α and t_β are introduced to account for the material softening caused by the temperature rise in α and β phases during post-yield deformations of the material. The variables s_α and s_β which did not vary with temperature in Mulliken and Boyce's constitutive equations are now functions of the present temperature and the present strain rate.

The presence of sub-β transitions in the polymer can be incorporated into the constitutive equations by adding an additional phase in parallel with the existing phases (cf. Fig. 8). Note that additional phases will have the same constitutive equations as those of α and β phases; only values of material parameters will differ.

It is *important* that the modified constitutive equations be validated for loadings other than the uniaxial compression (e.g. torsion, simple shear, uniaxial tension and multiaxial loading). However, this has not been accomplished here mainly due to the lack of test data for the same material.

Acknowledgements

This research was sponsored by the Army Research Laboratory and was accomplished under Cooperative Agreement Number W911NF-06-2-0014. The views and conclusions contained in this document are those of the authors and should not be interpreted as representing the official policies, either expressed or implied, of the Army Research Laboratory or the U.S. Government. The U.S. Government is authorized to reproduce and distribute reprints for Government purposes notwithstanding any copyright notation hereon.

Appendix A. Determination of material parameters

The modified constitutive equations require values of 16 material parameters. The determination of these material parameters from test data is a challenging task and may require several iterations of numerical simulations. The described techniques are applicable to glassy polymers and hence, details are given only for PC. Even though the material parameters introduced in the modified constitutive equations are strain softening parameters, we describe here techniques to determine both strain softening and strain hardening parameters. This is done since strain softening and strain hardening interact with each other. The determination of elastic constants, pressure coefficients, and yield parameters are described in Mulliken's thesis (Mulliken, 2004).

A.1. Determination of phase B parameters

The mechanical response of phase B is determined by two parameters – C_R and N_l. Phase B reproduces the strain hardening behavior observed in PC and PMMA and is dominant only at strains exceeding 30%. These material parameters cannot be computed directly and may require several iterations to converge to good values.

The axial stress vs. the axial strain plot from numerical simulations of the uniaxial compression test of phase B is generated for the iterative process. To simplify this computation, the deformation gradient in uniaxial compression at high strains is assumed to be of the form given in Eq. (20). The Cauchy stress in phase B during uniaxial loading can then be explicitly computed in terms of strains using Eq. (21).

Effects of varying C_R keeping N_l constant and varying N_l keeping C_R constant are shown in Fig. 26. It can be seen that reducing N_l causes the stress to increase exponentially at low strains. Also from Eq. (21), it can be seen that the stress varies linearly with C_R.

To determine material parameters for phase B, we iterate on C_R and N_l such that the slope of the true axial stress vs. the true axial strain curve computed using Eq. (21) is close to that of the experimental curve during uniaxial compression loading *in the strain hardening region*. An initial estimate of C_R = 15 MPa and N_l = 4 can be used. The result of this exercise is shown in Fig. 27 with experimental results corresponding to the strain hardening part of the curve and simulated results corresponding to the plot of Eq. (21). Note that in Fig. 27, the axial stress in phase B is plotted only in the strain hardening region (for strains greater than 30%).

A.2. Determination of material softening parameters

For the α and β phases, there are two softening parameters h_i and t_i^{ss} ($i = \alpha, \beta$). It is easier to first compute parameters for phase α based on results at low strain rates, since at high strain rates both

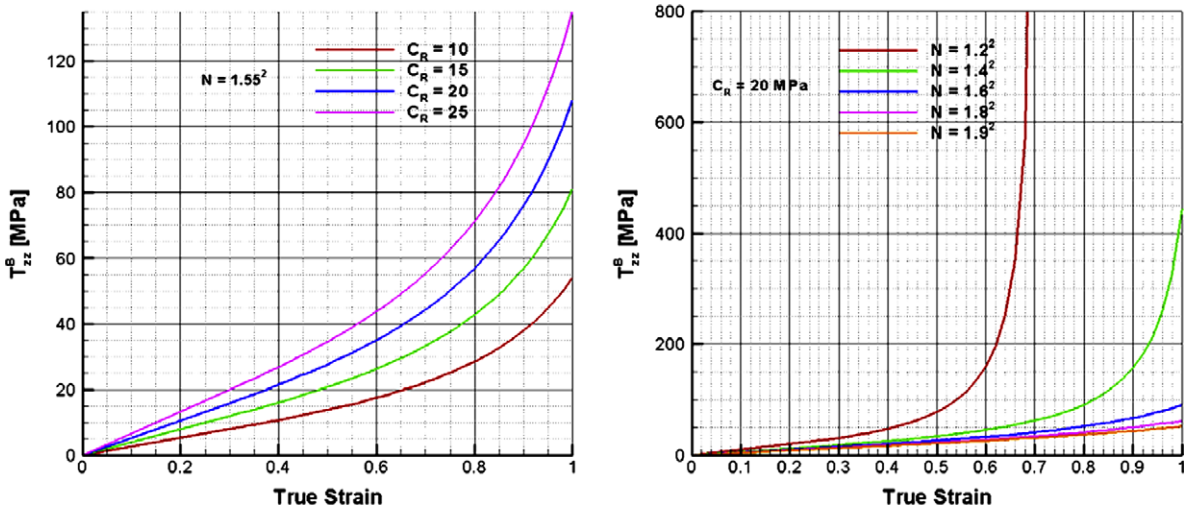

Fig. 26. Effect of material parameters on the axial stress vs. the axial strain curve of phase B; (a) effect of varying C_R keeping N_l constant, and (b) effect of varying N_l keeping C_R constant.

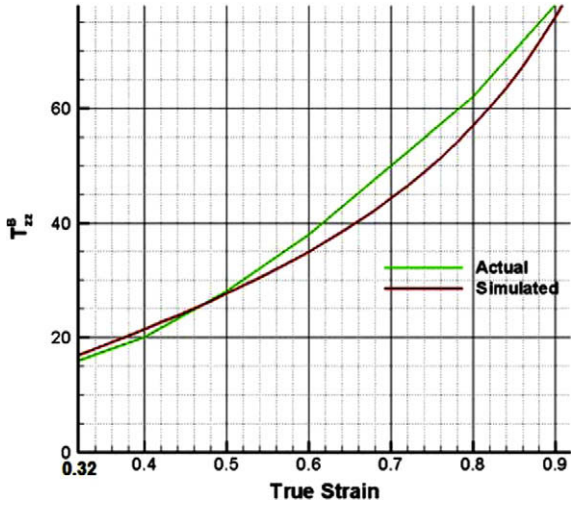

Fig. 27. Plot of the true axial stress in phase B vs. the true axial strain in uniaxial compression from experiments and simulations.

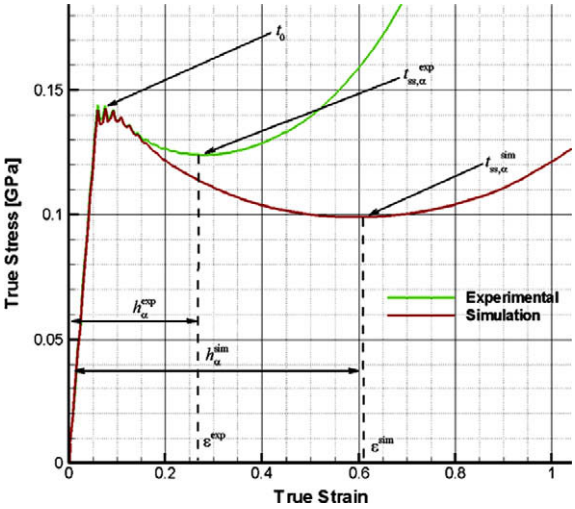

Fig. 28. Comparison of the true axial stress vs. the true axial strain plots from experiments and numerical simulations using an initial estimate of h_α.

α and β phases make comparable contributions. There is no direct method to compute these parameters and several iterations may be needed to converge to reasonable values of material parameters.

The parameter t^{ss}_α is a measure of the amount of softening in the material at low strain rates, while the parameter h_α is a measure of the rate at which softening occurs. An initial estimate of t^{ss}_α can be found from the ratio of the local minima in stress after yield to the yield stress (σ_{ss}/σ_y in Fig. 28). To determine the parameter h_α, a uniaxial compression test should be simulated using an initial estimate ($h_\alpha = 50$ MPa is suggested) of its value. Comparing the numerically computed true axial stress vs. true axial strain curve with the experimental one, a better estimate of h_α can be found from

$$h_\alpha = h^{sim}_\alpha \frac{\varepsilon^{exp}}{\varepsilon^{sim}} \tag{30}$$

Here, h^{sim}_α is the initial estimate of h_α, ε^{exp}, and ε^{sim} are the axial strains at which the local minima in the axial stress is achieved during experiments and simulations, respectively (cf. Fig. 28). In computing t^{ss}_α, it was assumed that only α phase contributes to stresses at yield and at the local minima. However, the magnitude of the axial stress at the axial strain of ε^{exp} is the sum of axial stresses from α and B phases (for low strain rates). Hence, to determine values of parameters t^{ss}_α and h_α, the iterative process needs to be repeated until the axial stress vs. the axial strain plots from experiments and numerical simulations at low strain rates match well with each other. It is equivalent to solving an inverse problem, i.e., find values of material parameters so that the computed axial stress vs. axial strain curve in uniaxial compression agrees well with the experimental one. This inverse technique of identifying values of material parameters was introduced in (Batra and Kim, 1990).

The method described for determining softening parameters for phase α can be applied to determine parameters for phase β as well. Values of softening parameters for phase α can be used as initial estimates of the values of softening parameters for phase β.

The material parameters determined for the proposed constitutive equations are given in Table 5 for PC and PMMA.

References

Arruda, E.M., Boyce, M.C., Jayachandran, R., 1995. Effects of strain rate, temperature and thermomechanical coupling on the finite strain deformation of glassy polymers. Mechanics of Materials 19, 193–212.

Batra, R.C., 2001. Comparison of results from four linear constitutive relations in isotropic finite elasticity. International Journal of Non-Linear Mechanics 36, 421–432.

Batra, R.C., Kim, C.H., 1990. Effect of viscoplastic flow rules on the initiation and growth of shear bands at high strain rates. Journal of the Mechanics and Physics of Solids 38, 859–874.

Batra, R.C., Adam, A., 1991. Effect of viscoplastic flow rules on steady state penetration of thermoviscoplastic targets. International Journal of Engineering Science 29, 1391–1408.

Batra, R.C., Jayachandran, R., 1992. Effect of constitutive models on steady state axisymmetric deformations of thermoelasto-viscoplastic targets. International Journal of Impact Engineering 12, 209–226.

Batra, R.C., Chen, L., 2001. Effect of viscoplastic relations on the instability strain, shear band initiation strain, the strain corresponding to the minimum shear band spacing, and the band width in thermoviscoplastic materials. International Journal of Plasticity 17, 1465–1489.

Bauwens-Crowet, C., 1973. The compression yield behavior of polymethyl-methacrylate over a wide range of temperatures and strain-rates. Journal of Materials Science 8, 968–979.

Bauwens-Crowet, C., Bauwens, J., Homes, G., 1972. The temperature dependence of yield of polycarbonate in uniaxial compression and tensile tests. Journal of Materials Science 7, 176–183.

Bodner, S., Partom, Y., 1975. Constitutive equations for elastic-viscoplastic strain-hardening materials. Journal of Applied Mechanics 42, 385–389.

Boyce, M.C., Arruda, E.M., 1990. An experimental and analytical investigation of the large strain compressive and tensile response of glassy polymers. Polymer Engineering and Science 30, 1288–1298.

Boyce, M.C., Parks, D., Argon, A., 1988. Large inelastic deformation of glassy polymers. Part I: rate dependent constitutive model. Mechanics of Materials 7, 15–53.

Chen, W., Lu, F., Cheng, M., 2002. Tension and compression tests of two polymers under quasi-static and dynamic loading. Polymer Testing 21, 113–121.

Eyring, H., 1963. Viscosity, plasticity, and diffusion as examples of absolute reaction rates. Journal of Chemical Physics 4, 283–295.

Fotheringham, D., Cherry, B.W., 1976. Comment on the compression yield behaviour of polymethyl methacrylate over a wide range of temperatures and strain-rates. Journal of Materials Science 11, 1368–1370.

Frank, G., Brockman, R., 2001. A viscoelastic–viscoplastic constitutive model for glassy polymers. International Journal of Solids and Structures 38, 5149–5164.

Garg, M., Mulliken, A.D., Boyce, M.C., 2008. Temperature rise in polymeric materials during high strain rate deformation. Journal of Applied Mechanics 75, 011009.

Haward, R., Thackray, G., 1968. The use of a mathematical model to describe the isothermal stress–strain curves in glassy thermoplastics. Proceedings of the Royal Society of London Series A, Mathematical and Physical Sciences 302, 453–472.

Ho, K., Krempl, E., 2002. Extension of the viscoplasticity theory based on overstress (VBO) to capture non-standard rate dependence in solids. International Journal of Plasticity 18, 851–871.

Krempl, E., Ho, K., 2000. Overstress model for solid polymer deformation behavior applied to Nylon 66. ASTM Special Technical Publication 1357, 118–140.

Lee, E.H., 1969. Elastic-plastic deformation at finite strains. Journal of Applied Mechanics 36, 1–6.

Leonov, A., Prokunin, A., 1994. Nonlinear Phenomena in Flows of Viscoelastic Polymer Fluids. Chapman & Hall, London.

Matsuoka, S., 1992. Relaxation Phenomena in Polymers. Hanser Publications, Munich.

Moy, P., Weerasooriya, T., Hsieh, A., Chen, W., 2003. Strain rate response of a polycarbonate under uniaxial compression. Proceedings of the SEM Conference on Experimental Mechanics.

Moy, P., Weerasooriya, T., Chen, W., Hsieh, A., 2003b. Dynamic stress–strain response and failure behavior of PMMA. ASME Applied Mechanics Division 254, 105–110.

Mulliken, A.D. 2004. Low to high strain rate deformation of amorphous polymers: experiments and modeling. M.Sc. Thesis (Mechanical Engineering). Massachusetts Institute of Technology, Cambridge.

Mulliken, A.D., Boyce, M.C., 2006. Mechanics of the rate-dependent elastic-plastic deformation of glassy polymers from low to high strain rates. International Journal of Solids and Structures 43, 1331–1356.

Parks, D., Argon, A., Bagepalli, B., 1984. Large Elastic-Plastic Deformation of Glassy Polymers. MIT Program in Polymer Science and Technology Report Massachusetts Institute of Technology, Boston.

Richeton, J., Ahzi, S., Vecchio, K.S., Jiang, F.C., Makradi, A., 2007. Modeling and validation of the large deformation inelastic response of amorphous polymers over a wide range of temperatures and strain rates. International Journal of Solids and Structures 44, 7938–7954.

Rittel, D., 1999. On the conversion of plastic work to heat during high strain rate deformation of glassy polymers. Mechanics of Materials 31, 131–139.

Treloar, L., 1975. The Physics of Rubber Elasticity. Clarendon, Oxford.

Varghese, A.G., 2008. Strain localization in tungsten heavy alloys and glassy polymers. Ph.D. Dissertation (Engineering Science and Mechanics). Virginia Polytechnic Institute and State University, Blacksburg.

Williams, M.L., Landel, R.F., Ferry, J.D., 1955. The temperature dependence of relaxation mechanisms in amorphous polymers and other glass-forming liquids. Journal of the American Chemical Society 77, 3701–3707.